Article

A forest biogeochemistry model intercomparison on the East Coast of the United States

Adam Erickson[1]*, Nikolay Strigul[1]

[1] Department of Mathematics and Statistics, Washington State University, 14204 NE Salmon Creek Avenue, Vancouver, WA 98686, USA; {adam.erickson, nick.strigul}@wsu.edu

* Correspondence: adam.erickson@wsu.edu; Tel.: +1-360-546-9655

Version November 30, 2018 submitted to Journal Not Specified

Abstract: Recent advances in forest ecosystem modeling allow the simulation of a suite of dynamics from site- to landscape-scale. In order to scale models efficiently from trees to landscapes, different model reduction strategies are employed. Yet, the results of these strategies and the assumptions they entail are rarely compared. Here, we conducted a model intercomparison exercise using two such forest biogeochemistry models, PPA-SiBGC and LANDIS-II NECN. We simulated past-decade conditions at flux tower sites in Harvard Forest, MA, USA and Jones Ecological Research Center, GA, USA. We mined the wealth of field data available for both sites to perform model parameterization, validation, and intercomparison. We assessed model performance using the following time-series metrics: net ecosystem exchange, aboveground net primary production, aboveground biomass, C, and N, belowground biomass, C, and N, soil respiration, and, species total biomass and relative abundance. We also assessed static observations of soil organic C and N, and concluded with an assessment of general model usability, performance, and transferability. Despite substantial differences in design, both models achieved good accuracy across the range of metrics. While LANDIS-II NECN performed better for interannual NEE fluxes due to its basis in the Century model, the PPA-SiBGC model indicated better overall correspondence to observational data for both sites across the 11 temporal and 2 static metrics tested (HF-EMS $\overline{R^2} = 0.73, +0.07$, $\overline{RMSE} = 4.84, -10.02$; JERC-RD $\overline{R^2} = 0.76, +0.04$, $\overline{RMSE} = 2.69, -1.86$).

Keywords: Perfect Plasticity Approximation; SORTIE-PPA; LANDIS-II; forest ecosystem simulation; forest biogeochemistry model; forest landscape model; model intercomparison; Harvard Forest; Jones Ecological Research Center

1. Introduction

Forest models are thought to have began 350 years ago in China with yield tables known as the Lung Ch'uan codes, invented by a women of the Kuo family in Suichuan county, Jiangxi [1]. It was not until the 20$^{\text{th}}$ century that the first complex mathematical models of forests emerged. Digital computers enabled researchers, for the first time, to explicitly model forest dynamics. Following the development of matrix models [2] and empirical growth-and-yield models such as Prognosis [3,4], a vast array of gap [5], forest landscape [6–10], and terrestrial biosphere models [11–13] have been developed. Models of forest ecosystems vary substantially in their representation of crown geometry and biogeochemical processes.

Representation of canopy geometry varies from implicit to a single 'big-leaf' and detailed three-dimensional crown and root geometry (e.g., modern gap models such as MAESPA [14] and LES [15]). Models of growth range from simple allometric equations (e.g., growth-and-yield models) to light-use efficiency models [16] and first-principles mechanistic models of photosynthesis [17]. Belowground process models similarly vary in structure, from simple stoichiometric relations to carbon and nitrogen cycling with microbial dynamics to a fully mechanistic representation of energetic and biogeochemical processes based on thermodynamics. Current belowground models vary considerably in their process representation and accuracy, with much improvement left to be made [18]. Most belowground models in use globally rely on a variant of the classical Century model [19,20].

Model specialization and generalization ranges from pure research applications in narrowly defined areas (e.g., [14]) to simulating multiple loosely coupled landscape processes to simulating biogeochemical fluxes throughout the world's forests. A trade-off is thought to exist between realism, precision, and generality [21], with more detailed models requiring higher parameterization costs. Yet, little is known about the net effects of variation in the structure of these models on the precision and accuracy of their predictions across temporal and spatial scales. While such model intercomparisons are common within classes of models such as terrestrial biosphere models, they are seldom applied to gap or forest landscape models. Models operating at different scales are seldom compared within sites. Yet, much can be learned by comparing models that differ in assumptions and structure.

Existing forest model intercomparison projects, or MIPs, in Europe include the stand-level Intersectoral Impact MIP (ISIMIP) [22] and landscape-level Comparison of Forest Landscape Models (CoFoLaMo) [23], the latter conducted under the European Union Cooperation on Science and Technology (COST) Action FP1304 "Towards robust projections of European forests under climate change" (ProFoUnd). Previous efforts in the United States include the Throughfall Displacement Experiment (TDE) Ecosystem Model Intercomparison Project at Walker Branch Watershed in Oak Ridge, Tennessee [24]. Presently, no other forest model intercomparison project is evident for North America. There is a critical need to conduct ongoing forest biogeochemistry model comparisons in this and other regions of the world in order to establish the regional foundation for robust global C cycle projections. In this work, we aim to begin this process for North America with a comparison of the Perfect Plasticity Approximation with Simple Biogeochemistry (PPA-SiBGC) and Landscape Disturbance and Succession with Net Ecosystem Carbon and Nitrogen (LANDIS-II NECN) models, which provide contrasting model structures for representing stand dynamics.

Modern forest landscape models are the result of five key model development phases, listed in chronological order: (1) growth-and-yield models; (2) fire models; (3) gap models; (4) physiological models; (5) hybrid models combining design principles from each [5,25,26]. Terrestrial biosphere models similarly trace their roots back to early one-dimensional physiological models, with land surface models currently in their third generation and dynamic global vegetation models in their second generation [27]. This latest generation of models was intended to address the lack of explicit representation of vegetation dynamics - a critical source of model uncertainty in future climate scenarios [28]. This inspired the aforementioned forest ecosystem model intercomparisons as well as new terrestrial biosphere model designs based on gap models, bypassing the trade-offs of medium-resolution forest landscape models.

Collectively, these efforts yielded a number of new terrestrial biosphere models based on the classical gap model, including the Lund-Potsdam-Jena General Ecosystem Simulator (LPJ-GUESS) [29], the Ecosystem Demography model (ED/ED2) [30,31], and Land Model 3 with PPA (LM3-PPA) [32], based on the Perfect Plasticity Approximation (PPA) [33,34]. These models represent the current state-of-the-art in modeling vegetation dynamics globally. While individual-based global models have begun to merge, forest landscape models have remained in between, focused on spatial processes of fire, harvest, and biological disturbance. Yet, previous research has shown that such forest landscape models are often insensitive to landscape configuration and are therefore aspatial [35], counter to the main assumption and selling point of these models.

While most forest landscape and terrestrial biosphere models lack individual trees, the SAS [30] and PPA [33,36,37] model reduction strategies have demonstrated an ability to successfully up-scale gap dynamics to forest stands. Other up-scaling strategies exist as well. One recent forest landscape model participating in the CoFoLaMo intercomparison scales from individual trees to stands by pre-computing light tables [38]. Regardless of the model structure, it is clear that gap, forest landscape, and terrestrial biosphere models are beginning to merge into new models of the terrestrial biosphere. This trend is also attributable to improvements in computational efficiency with new processor designs and cluster or cloud computing infrastructure. As few, if any, existing models are designed for highly parallel architectures (e.g., general-purpose graphics processing units, or GPGPUs), there remains much potential for future model efficiency gains.

In this forest biogeochemistry model intercomparison, we focus on two sites on the East Coast of the United States, Harvard Forest (HF), Massachusetts and Jones Ecological Research Center (JERC), Georgia. The two sites were selected for their representativeness of the United States Eastern Seaboard and for the availability of data needed to parameterize and validate the models. Harvard Forest is one of the most-studied forests in the world, with Google Scholar returning 12,700 results for the site. We focus on results for the Environmental Measurement Station (EMS) eddy covariance (EC) flux tower site within the Little Prospect Hill tract - the longest-running eddy covariance flux tower in the world. Previous research at the EMS EC flux tower site found unusually high rates of ecosystem respiration in winter and low rates in mid-to-late summer compared to other temperate forests [39]. While the mechanisms behind these observed patterns remains poorly understood, this observation is outside the scope of the presented research.

Between 1992 and 2004, the site acted as a net carbon sink, with a mean annual uptake rate of $2.5 MgCha^{-1}year^{-1}$. Aging dominated the site characteristics, with a 101-115 Mg C ha-1 increase in biomass, comprised predominantly of growth of red oak (*Quercus rubra*). The year 1998 showed a sharp decline in net ecosystem exchange (NEE) and other metrics, recovering thereafter [40]. As Urbanski *et al.* [40] note of the Integrated Biosphere Simulator 2 (IBIS2) and similar models at the time, "the drivers of interannual and decadal changes in NEE are long-term increases in tree biomass, successional change in forest composition, and disturbance events, processes not well represented in current models." The two models used in the intercomparison study, a SORTIE-PPA [33,34] variant and LANDIS-II with NECN succession [41,42], are intended to directly address these model shortcomings.

While there have been fewer studies at Jones Ecological Research Center, Georgia, USA, Google Scholar returns 1,370 results for the site, reflecting its growing role in forest sciences research. Our study focuses on the Red Dirt (RD) EC flux tower site within the mesic sector, for which a handful of relevant studies exist. Two recent studies [43,44] indicate that the mesic sector of this subtropical pine savanna functions as a moderate carbon sink (NEE = $-0.83\, Mg\, C\, ha^{-1}\, year^{-1}$; $-1.17\, Mg\, C\, ha^{-1}\, year^{-1}$), reduced to near-neutral uptake during the 2011 drought (NEE = $-0.17\, Mg\, C\, ha^{-1} year^{-1}$), and is a carbon source when prescribed burning is taken into account. NEE typically recovered to pre-fire rates within 30-60 days. The mechanisms behind soil respiration rates here again appear to be complex, site-specific, and poorly understood [44].

Overall, existing research highlights the importance of fire and drought to carbon exchange in long-leaf pine (*Pinus palustris*) and oak (*Quercus spp.*) savanna systems [43–45] at JERC. This is in contrast to the secondary growth-dominated deciduous broadleaf characteristics of Harvard Forest. Species diversity at the EMS tower site is 350% greater than that of the JERC-RD site, with 14 species from a variety of genera compared to four species from only two genera, *Pinus* and *Quercus*.

In this work, we aim to establish a foundation for future forest biogeochemistry model intercomparisons. This includes open-source object-oriented software to facilitate model parameterization, validation, intercomparison, and simplified reproducibility of results. We perform the model intercomparison for two key research forests in the United States to assess the ability of each model to reproduce observed biogeochemistry pools and fluxes over time. We hypothesize that the inclusion of forest growth, compositional change, and mortality processes in both models will allow for accurate predictions of biomass and NEE dynamics, as suggested in previous research Urbanski *et al.* [40]. Accordingly, we compare both models to observations and to each other for a host of metrics related to biomass, C, N, and forest composition at the two research sites.

2. Materials and Methods

LANDIS-II NECN and PPA-SiBGC were parameterized for two forested sites in the eastern United States, Harvard Forest, Massachusetts and Jones Ecological Research Center, Georgia. At the HF site, we focus on Little Prospect Hill and the EMS EC flux tower (HF-EMS). At the JERC site, we focus on the mesic zone and RD EC flux tower (JERC-RD). Both sites provided local EC and meteorological measurements to conduct this study. Plots of EC flux and meteorological tower measurements for both sites are located in Appendix A; maps of both sites are located in Appendix B.

Both models were parameterized using data available for each site, including local (i.e., field measurements) and general information sources (e.g., species compendiums and other published sources). As these empirical or observational values were used to parameterize both models, further model calibration (i.e., parameter tuning) was not necessary. This is because tuning parameters away from measured values to improve model performance, or defining a separate set of tuning parameters, is known to produce model over-fitting (i.e., reduced generality) and thus false improvements in model accuracy through reduced parsimony [46]. We explicitly avoided this practice, as it is only appropriate when fitting empirical growth-and-yield models such as Prognosis, also known as the Forest Vegetation Simulator (FVS) [3,4]. All model parameters are provided in the Appendix C. We close the methodology section with descriptions of the metrics, models, and criteria used in the intercomparisons.

2.1. Model Descriptions

In the following sections, we provide a brief overview of the two forest ecosystem models used in this intercomparison study. For detailed information on each model, readers are encouraged to refer to the original publications.

2.1.1. LANDIS-II NECN

The LANDIS-II model is an extension of the original LANdscape DIsturbance and Succession (LANDIS) model [47–49] into a modular software framework [41]. Specifically, LANDIS-II is a model core containing basic state information that interfaces or communicates with external user-developed models known as "extensions" using a combination of object-oriented and modular design. This design makes LANDIS-II a modeling framework rather than a model. The LANDIS family of models, which also includes LANDIS PRO [50] and Fin-LANDIS [51,52], are stochastic hybrid models [25] based on the vital attributes/fuzzy systems approach of the LANDSIM model genre [53]. Perhaps unknowingly, this genre borrows heavily from cellular automata [54] and thus Markov Chains by applying simple heuristic rule-based systems, in the form of vital attributes, across two-dimensional grids.

Models of the LANDSIM genre focus on landscape-scale processes and assume game-theoretic vital attribute controls over successional trajectories following disturbance [55]. The LANDSIM model genre is thus a reasonable match for the classical forest fire model [56], given its local two-dimensional cellular basis. In contrast to the original LANDIS model, LANDIS-II is implemented in Microsoft C# rather than ISO C++98 [57], simplifying model development in exchange for a proprietary single-vendor software stack [41].

The latest version of LANDIS-II (v7) supports Linux through use of the Microsoft .NET Core developer platform. The modular design of LANDIS-II is intended to simplify the authorship and interaction of user-provided libraries for succession and disturbance. The centralized model core stores basic landscape and species state information and acts as an interface between succession and disturbance models. While there have been numerous forest landscape models over the years [6–10], the LANDIS family of models has enjoyed notable longevity and is currently united under the LANDIS-II Foundation. Part of its longevity is attributable to the prioritization of model functionality over realism in order to appeal to application-minded managers seeking a broad array of functionality.

The Net Ecosystem Carbon and Nitrogen (NECN) model [42] is a simplified variant of the classical Century model [19,20]. The original ten soil layers in Century have been replaced by a single soil layer, with functions for growth and decay borrowed directly from Century v4.5. The NECN succession model Figure 1 is thus a process-based model that simulates C and N dynamics along the plant-soil continuum at a native monthly timestep.

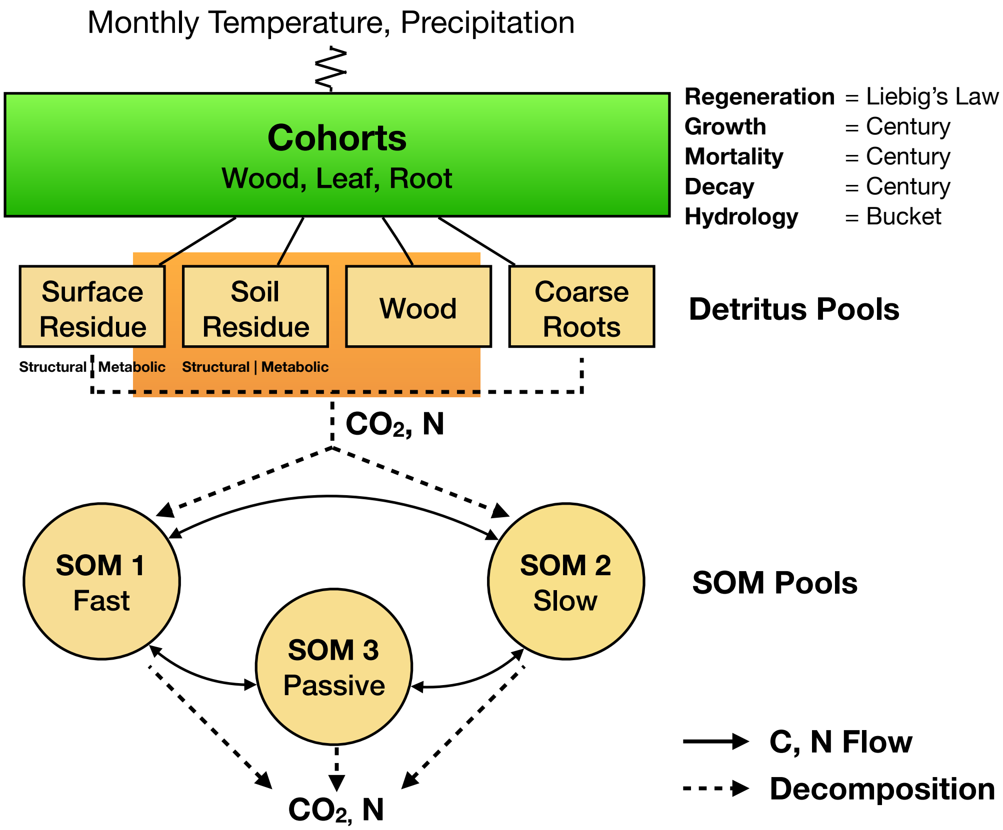

Figure 1. LANDIS-II NECN model structure

Atmospheric effects are included through monthly climate (i.e., temperature maxima, minima, means, and standard deviations, and precipitation means and standard deviations). Explicit geometric representation of tree canopies is forgone in favor of bounded statistical growth models based theoretically on Liebig's Law of the Minimum. Functions for growth, mortality, and decay are adopted from Century [19] while hydrology is based on the simple bucket model [58]. The regeneration function is the only new process in NECN and is also based on Liebig's Law. For a detailed description of the NECN model, readers may refer to the original model publication [42]. Parameterization of the LANDIS-II model for both sites was based on updating parameters used in recent [59–62] and ongoing (Flanagan et al., *in review*) work.

2.1.2. PPA-SiBGC

The PPA-SiBGC model belongs to the SORTIE-PPA family of models [33,36] within the SAS-PPA model genre, based on a simple and analytically tractable approximation of the classical SORTIE gap model [63,64]. The Perfect Plasticity Approximation, or PPA [33,34], was derived from the dual assumptions of perfect crown plasticity (e.g., space-filling) and phototropism (e.g., stem-leaning), both of which were supported in empirical and modeling studies [36]. The discovery of the PPA was rooted in extensive observational and *in silico* research [33]. The PPA model was designed to overcome the most computationally challenging aspects of gap models in order to facilitate model scaling from the landscape to global scale.

The PPA and its predecessor, the size-and-age structured (SAS) equations [30,65], are popular model reduction techniques employed in current state-of-the-art terrestrial biosphere models [13]. The PPA model can be thought of metaphorically as Navier-Stokes equations of forest dynamics, capable of modeling individual tree population dynamics with a one-dimensional von Foerster partial differential equation [33]. The simple mathematical foundation of the PPA model is provided in Equation 1.

$$1 = \int_{z^*}^{\infty} \sum_{j=1}^{k} N_j(z) A_j(z^*, z) dz \tag{1}$$

where k is the number of species, j is the species index, $N_j(z)$ is the density of species j at height z, $A_j(a^*, z)$ is the projected crown area of species j at height z, and dz is the derivative of height. In other words, we discard the spatial location of individual trees and calculate the height at which the integral of tree crown area is equal to the ground area of the stand. This height is known as the theoretical z^* height, which segments trees into overstory and understory classes [33].

The segmentation of the forest canopy into understory and overstory layers allows for separate coefficients or functions for growth, mortality, and fecundity to be applied across strata, whose first moment accurately approximates the dynamics of individual-based forest models. Recent studies have shown that the PPA model faithfully reduces the dynamics of the more recent neighborhood dynamics (ND) SORTIE-ND gap model [66] and is capable of accurately capturing forest dynamics [67,68].

In this work, we applied a simple biogeochemistry variant of the SORTIE-PPA model, PPA-SiBGC [Erickson and Strigul, *In Review*] Figure 2.

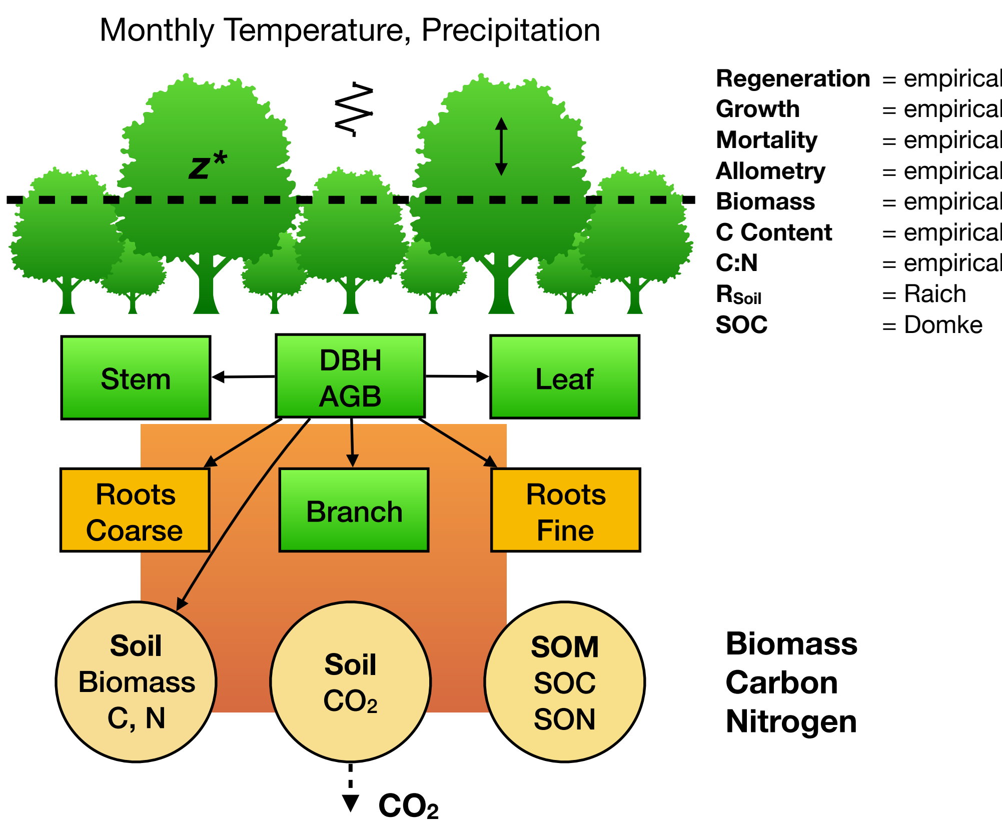

Figure 2. PPA-SiBGC model structure; Raich *et al.* [69]; Domke *et al.* [70]

Empirical observations were relied upon for the C and N content of tree species compartments. Stoichiometric relations were used to estimate N from C, based on empirical measurements provided for both sites. All values were calculated directly from observations. Previously published equations [71] and parameters [72] were used to model crown allometry. Together with inventory data, general biomass equations were used to estimated dry weight mass (*kg*) for tree stems, branches, leaves, and, fine and coarse roots [73]. Carbon content is assumed to be 50% of dry mass, supported by data. Monthly soil respiration is modeled using the approach of Raich *et al.* [69], while soil organic C is modeled using the simple generalized approach of Domke *et al.* [70]. Species- and stratum-specific parameters for growth, mortality, and fecundity were calculated from observational data available for both sites.

2.2. Site Descriptions

In the following sections, we describe the two forested sites on the East Coast of the United States: HF-EMS and the JERC-RD. A critical factor in the selection of the sites was the availability of eddy covariance flux tower data needed to validate NEE in the models.

2.2.1. HF-EMS

The HF-EMS EC flux tower is located within the Little Prospect Hill tract of Harvard Forest (42.538°N, 72.171°W, 340 m elevation) in Petersham, Massachusetts, approximately 100 km from the city of Boston [40]. The tower has been recording NEE, heat, and meteorological measurements since 1989, with continuous measurements since 1991, making it the longest-running eddy covariance measurement system in the world. The site is currently predominantly deciduous broadleaf second-growth forests approximately 75-95 years in age, based on previous estimates [74]. Soils at Harvard Forest originate from sandy loam glacial till and are reported to be mildly acidic [40].

The site is dominated by red oak (*Quercus rubra*) and red maple (*Acer rubrum*) stands, with sporadic stands of Eastern hemlock (*Tsuga canadensis*), white pine (*Pinus strobus*), and red pine (*Pinus resinosa*). When the site was established, it contained 100 Mg C ha^{-1} in live aboveground woody biomass [74]. As noted by Urbanski *et al.* [40], approximately 33% of red oak stands were established prior to 1895, 33% prior to 1930, and 33% before 1940. A relatively hilly and undisturbed forest (since the 1930s) extends continuously for several km^2 around the tower. In 2000, harvest operations removed 22.5 Mg C ha^{-1} of live aboveground woody biomass about 300 m S-SE from the tower, with little known effect on the flux tower measurements. The 40 biometric plots were designated via stratified random sampling within eight 500 m transects Urbanski *et al.* [40]. The HF-EMS tower site currently contains 34 biometric plots at 10 m radius each, covering 10,681 m^2, or approximately one hectare, in area. Summary statistics for the EMS tower site are provided in Table 1.

Table 1. HF-EMS site forest inventory summary; DBH in cm and aboveground biomass (B_{AG}) in kg

Statistic	N	Mean	St. Dev.	Min	Pctl(25)	Pctl(75)	Max
Year	7,234	2006.93	3.155	2002	2004	2010	2012
DBH	7,234	24.79	11.63	9.60	15.53	32.37	72.40
B_{AG}	7,234	385.90	507.07	22.50	88.82	470.28	4,216.27

A table of observed species abundances for the 2002-2012 period are provided in Table 2.

Table 2. HF-EMS site species abundance

Species	Count
ACPE	6
ACRU	2720
BEAL	400
BELE	131
BEPO	64
FAGR	152
FRAM	143
PIGL	251
PIRE	342
PIST	334
PRSE	150
QURU	1366
QUVE	135
TSCA	1012

Data were collected here for a range of studies, as evidenced by the Harvard Forest Data Archive. Datasets used in model validation include HF001-04, HF004-02, HF069-09, HF278-04, HF069-06, HF015-05, HF006-01, and HF069-13. These include weather station and forest inventory time-series, eddy covariance flux tower measurements, soil respiration, soil organic matter, and studies on C:N stoichiometry. Standard measurement techniques were used for each. For both sites, local tree species, age, depth-at-breast-height (DBH), biomass, soil, and meteorological data were primarily used to parameterize the models.

2.2.2. JERC-RD

Jones Ecological Research Center at Ichauway is located near Newton, Georgina, USA (31°N, 84°W, 25-200 m elevation). The site falls within the East Gulf Coastal Plain and consists of flat to rolling land sloping to the southwest. The region is characterized by a humid subtropical climate with temperatures ranging from 5-34 °C and precipitation averaging 132 cm year-1. The overall site is 12,000 ha in area, 7,500 ha of which are forested [75]. The site also exists within a tributary drainage basin that eventually empties into the Flint River. Soils here are underlain by karst Ocala limestone and mostly Typic Quartzipsamments, with sporadic Grossarenic and Aquic Arenic Paleudults [76]. Soils here often lack well-developed organic horizons [75–77].

Forests here are mostly second-growth, approximately 65-95 years in age. Long-leaf pine (*Pinus palustris*) dominates the overstory, while the understory is comprised primarily of wiregrass (*Aristida stricta*) and secondarily of shrubs, legumes, forbs, immature hardwoods, and regenerating long-leaf pine forests [78]. Prescribed fire is a regular component of management here, with stands often burned at regular 1-5 year intervals [75]. This has promoted wiregrass and legumes in the understory, while reducing the number of hardwoods [75]. The RD EC flux tower is contained within the mesic/intermediate sector. This site consists of only four primary tree species from two genera: long-leaf pine (*Pinus palustris*), water oak (*Quercus nigra*), southern live oak (*Quercus virginiana*), and bluejack oak (*Quercus incana*). Measurements for the RD tower are available for the 2008-2013 time period. Summary statistics for the RD tower site are provided in Table 3.

Table 3. JERC-RD site forest inventory summary; DBH in cm and aboveground biomass (B_{AG}) in kg

Statistic	N	Mean	St. Dev.	Min	Pctl(25)	Pctl(75)	Max
Year	1,012	2011.01	1.42	2009	2010	2012	2013
DBH	1,012	31.10	12.73	10.70	18.96	42.25	62.75
B_{AG}	1,012	707.28	564.65	3.91	177.27	1,179.59	2,708.08

A table of observed species abundances for the 2009-2013 period are provided in Table 4.

Table 4. JERC-RD site species abundance

Species	Count
PIPA	967
QUIN	5
QUNI	10
QUVI	30

Datasets used in model validation at JERC-RD include JC010-02, JC010-01, JC003-04, JC004-01, JC003-07, and JC011-01. These include weather station and eddy covariance flux tower measurements, forest inventory data, soil respiration, soil organic matter, and studies on C:N stoichiometry. Standard measurement techniques were also used for each of these.

2.3. Site Data

To conduct this model intercomparison exercise at HF-EMS, we leveraged the large amount of data openly available to the public through the Harvard Forest Data Archive:

http://harvardforest.fas.harvard.edu/harvard-forest-data-archive

Jones Ecological Research Center has hosted multiple research efforts over the years, collectively resulting in the collection of a large data library. However, JERC-RD site data are not made openly available to the public and are thus only available by request. One may find contact information located within their website:

http://www.jonesctr.org

2.4. Scales, Metrics, and Units

The selection of simulation years was based on the availability of EC flux tower data used in model validation. Thus, we simulated the HF-EMS site for the years 2002-2012 and the JERC-RD site for the years 2009-2013. For both sites and models, we initialized the model state in the first year of simulations using field observations. The PPA-SiBGC model used an annual timestep while LANDIS-II NECN used a monthly timestep internally. Both models may be set to other timesteps if desired.

The areal extent of the single-site model intercomparisons were designed to correspond to available field measurements. At both sites, tree inventories were conducted in 10,000 m^2, or one-hectare, areas. All target metrics were converted to an annual areal basis to ease interpretation, comparison, and transferability of results. Importantly, an areal conversion will allow comparison to other sites around the world. While flux tower measurements for both sites were already provided on an areal (m^{-2}) basis, many other variables were converted to harmonize metrics between models and study sites. For example, moles CO_2 measurements were converted to moles C through well-described molecular weights, all other measures of mass were converted to kg, and all areal and flux measurements were harmonized to m^{-2}. A table of metrics and units used in the intercomparison of LANDIS-II and PPA-SiBGC is provided in Table 5.

Table 5. Model intercomparison abbreviations, metrics, and units

Abbreviation	Metric	Units
NEE	Net ecosystem exchange	$kg\ C\ m^{-2}\ year^{-1}$
B_{AG}	Aboveground biomass	$kg\ mass\ m^{-2}$
C_{AG}	Aboveground C	$kg\ C\ m^{-2}$
N_{AG}	Aboveground N	$kg\ N\ m^{-2}$
B_{BG}	Belowground biomass	$kg\ mass\ m^{-2}$
C_{BG}	Belowground C	$kg\ C\ m^{-2}$
N_{BG}	Belowground N	$kg\ N\ m^{-2}$
C_{SO}	Soil organic C	$kg\ C\ m^{-2}$
N_{SO}	Soil organic N	$kg\ N\ m^{-2}$
r_{soil}	Soil respiration C	$kg\ C\ m^{-2}\ year^{-1}$
ANPP	Aboveground net primary production	$kg\ mass\ m^{-2}\ year^{-1}$
B_{Sp}	Species aboveground biomass	$kg\ mass\ m^{-2}$
n_{Sp}	Species relative abundance	%

In the subsequent section, we describe the model intercomparison methodology.

2.5. Model Intercomparison

Intercomparison of the PPA-SiBGC and LANDIS-II models at the HF-EMS and JERC-RD EC flux tower sites was conducted using a collection of object-oriented functional programming scripts written in the R language for statistical computing [79]. These scripts were designed to simplify model configuration, parameterization, operation, calibration/validation, plotting, and error calculation. The scripts and our parameters are available on GitHub (https://github.com/adam-erickson/ecosystem-model-comparison), making our results fully and efficiently reproducible. The R scripts are also designed to automatically load and parse the results from previous model simulations, in order to avoid reproducibility issues stemming from model stochasticity. We use standard regression metrics applied to the time-series of observation and simulation data to assess model fitness. The metrics used include the coefficient of determination (R^2), root mean squared error (RMSE), mean absolute error (MAE), and mean error (ME) or bias, calculated using simulated and observed values. Our implementation of R^2 follows the Bravais-Pearson interpretation as the squared correlation coefficient between observed and predicted values [80]. This implementation is provided in Equation 2.

$$R^2 = r^2 = \left(\frac{\sum_{i=1}^{n} (y_i - \overline{y})(\hat{y}_i - \overline{\hat{y}})}{\sqrt{\sum_{i=1}^{n} (y_i - \overline{y})^2 (\hat{y}_i - \overline{\hat{y}})^2}} \right)^2 \tag{2}$$

where n is the sample size, y_i is the ith observed value, $\hat{y}_i$ is the ith predicted value, $\overline{y}$ is the mean observed value, and $\overline{\hat{y}}$ is the mean predicted value. The calculation of RMSE follows the standard formulation, as shown in Equation 3.

$$RMSE = \sqrt{\frac{1}{n} \sum_{t=1}^{n} e_t^2} \tag{3}$$

where n is the sample size and e_t is the error for the tth value, or the difference between observed and predicted values. The calculation of MAE is similarly unexceptional, per Equation 4.

$$MAE = \frac{1}{n} \sum_{t=1}^{n} |e_t| \tag{4}$$

where again n is the sample size and e_t is the error for the tth value. Our calculation of mean error (ME) or bias is the same as MAE, but without taking the absolute value.

While Nash-Sutcliffe efficiency (NSE) is often used in a simulation model context, we selected the Bravais-Pearson interpretation of R^2 over NSE to simplify the interpretation of results. The NSE metric replaces $1 - (SS_{predictions}/SS_{observations})$ with $(SS_{observations} - SS_{predictions})/SS_{observations}$, where SS is the sum of squares. Thus, NSE is analogous to the standard R^2 coefficient of determination used in regression analysis [81]. The implementation of R^2 that we selected is important to note, as its results are purely correlative and quantify only dispersion, ranging in value between 0 and 1. This has some desirable properties in that no negative or large values are produced, and that it is insensitive to differences in scale. Regardless of the correlation metric used, complementary metrics are needed to quantify the direction (i.e., bias) and/or magnitude of error. We rely on RMSE and MAE to provide information on error or residual magnitude, and ME to provide information on bias. We utilize a visual analysis to assess error directionality over time, as this can be poorly characterized by a single coefficient, masking periodicity.

We compute R^2, RMSE, MAE, and ME for time-series of the metrics described in Table 5 on page 10. These include NEE, above- and below-ground biomass, C, and N, soil organic C and N, soil respiration (r_{soil}), aboveground net primary production (ANPP), and, species aboveground biomass and relative abundance. All of these metrics are pools with the exception of NEE, r_{soil}, and ANPP fluxes. Finally, we diagnose the ability of both models to meet a range of logistical criteria related to deployment: *model usability, performance, and transferability*. Model usability is assessed per four criteria:

1. Ease of installation
2. Ease of parameterization
3. Ease of program operation
4. Ease of parsing outputs

Model software performance is assessed per a single metric: the speed of program execution for each site for the predefined simulation duration. The durations are 11 years and 5 years for the HF-EMS and JERC-RD EC flux tower sites, respectively. Simulation results are output at annual temporal resolution, the standard resolution for both models; while NECN operates on a monthly timestep, most other modules of LANDIS-II are annual. Finally, model transferability is assessed per the following five criteria:

1. Model generalizability
2. Availability of parameterization data
3. Size of the program
4. Cross-platform support
5. Ease of training new users

Each of these logistical criteria are compared in a qualitative analysis, with the exception of software performance.

3. Results and Discussion

Both PPA-SiBGC and LANDIS-II NECN showed strong performance for pools at the two model intercomparison sites, frequently achieving R^2 values approaching unity. Yet, both models showed weak performance for fluxes. The models failed to accurately predict ANPP, while PPA-SiBGC showed stronger r_{soil} performance and LANDIS-II NECN showed stronger NEE performance. The R^2 values for both models and sites are visualized in Figure 3.

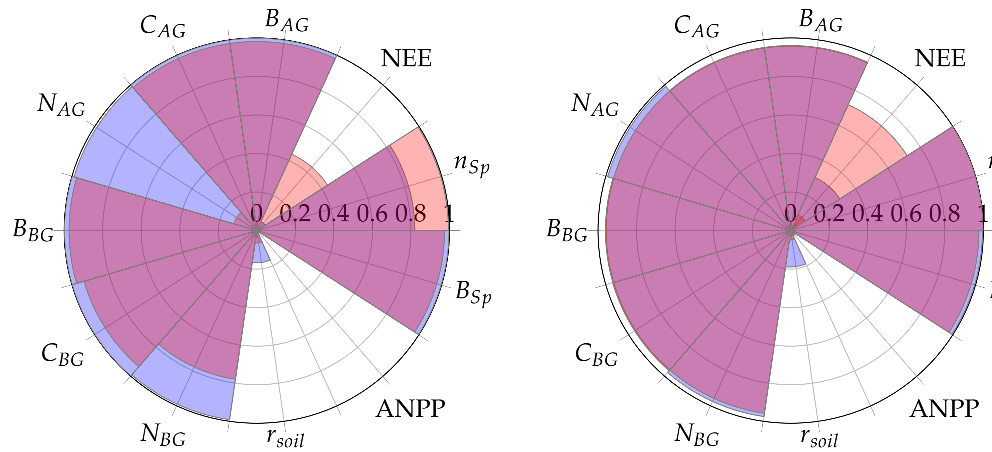

Figure 3. Overall model performance (R^2) for both models and sites; *left = HF-EMS; right = JERC-RD; periwinkle = PPA-SiBGC; pink = LANDIS-II NECN; violet = intersection*

On average, PPA-SiBGC outperformed LANDIS-II NECN across the sites and metrics tested, showing higher correlations, lower error, and less bias overall (HF-EMS $\overline{R^2} = 0.73, +0.07$, $\overline{RMSE} = 4.84, -0.39$, $\overline{ME} = -1.18, -3.70$; JERC-RD $\overline{R^2} = 0.76, +0.04$, $\overline{RMSE} = 2.69, -0.17$, $\overline{ME} = 0.78, +0.53$). This result is based on calculating mean values for R^2, RMSE, MAE, and ME in order to clearly translate the overall results. The two models produced the following mean values for each of the four statistical metrics and two sites:

Table 6. Overall mean values across each of the sites and metrics tested

	PPA-SiBGC				LANDIS-II NECN			
Metric	R^2	RMSE	MAE	ME	R^2	RMSE	MAE	ME
Mean	0.74	3.77	3.58	-0.20	0.69	9.60	8.73	2.31

As shown in Table 6, PPA-SiBGC yielded higher R^2 values and lower RMSE, MAE, and ME values in comparison to LANDIS-II, on average, across all sites and metrics tested. Below, we provide model intercomparison results individually for the two sites, HF-EMS and JERC-RD.

3.1. HF-EMS

For the HF-EMS site, PPA-SiBGC showed higher R^2 values and lower RMSE, MAE, and ME values compared to LANDIS-II NECN across the range of metrics. While PPA-SiBGC predicted NEE and species relative abundance showed weaker correlations with observed values compared to LANDIS-II NECN, the magnitude of error was lower, as evidenced by lower RMSE, MAE, and ME values. While LANDIS-II NECN showed a lower magnitude of error for belowground N, this is the only metric where this is the case, while the correlation of this metric to observed values was also lower than that of PPA-SiBGC. Overall results for the HF-EMS site model intercomparison are shown in Table 7.

Table 7. Model fitness for HF-EMS

	PPA-SiBGC				LANDIS-II NECN			
Metric	R^2	RMSE	MAE	ME	R^2	RMSE	MAE	ME
NEE	0.05	0.19	0.16	-0.03	0.44	0.49	0.44	0.44
B_{AG}	1.00	10.12	10.11	10.11	0.98	2.48	2.48	-2.48
C_{AG}	1.00	0.03	0.03	-0.02	0.98	1.24	1.24	-1.24
N_{AG}	0.99	1.44	1.44	-1.44	0.12	1.99	1.99	-1.99
B_{BG}	1.00	9.09	9.08	9.08	0.97	2.82	2.82	-2.82
C_{BG}	1.00	7.82	7.81	-7.81	0.93	9.87	9.86	-9.86
N_{BG}	0.99	0.56	0.56	0.56	0.78	0.12	0.12	-0.12
r_{soil}	0.17	0.63	0.62	-0.62	0.06	1.10	1.10	-1.10
ANPP	0.02	0.20	0.20	-0.20	0.0002	0.82	0.79	0.73
C_{SO}	...	26.49	26.49	-26.49	...	36.63	36.63	-36.63
N_{SO}	...	1.33	1.33	-1.33	...	1.60	1.60	-1.60
B_{Sp}	1.00	5.02	2.89	2.89	0.97	133.70	119.87	119.87
n_{Sp}	0.82	0.05	0.03	0	0.99	0.29	0.22	0.22
Mean	0.73	4.84	4.67	-1.18	0.66	14.86	13.78	4.88

Time-series figures allow a visual analysis of the temporal dynamics between observations and model predictions in order to assess the ability of models to capture interannual variability. Both models effectively captured temporal dynamics in biomass, C, and, species biomass and abundance. In Figure 4, the temporal differences in modeled NEE and aboveground C are shown for the two models in comparison to observations for the HF-EMS site. While LANDIS-II NECN predicted NEE showed a higher correlation with observations, the magnitude of error and bias were also higher. Furthermore, LANDIS-II NECN predicted that the HF-EMS site is a net C source, rather than sink, in contrary to observations. Meanwhile, PPA-SiBGC outperformed LANDIS-II NECN in aboveground C per both R^2 and RMSE. Both models overpredicted species cohort biomass, while LANDIS-II NECN underpredicted total aboveground C.

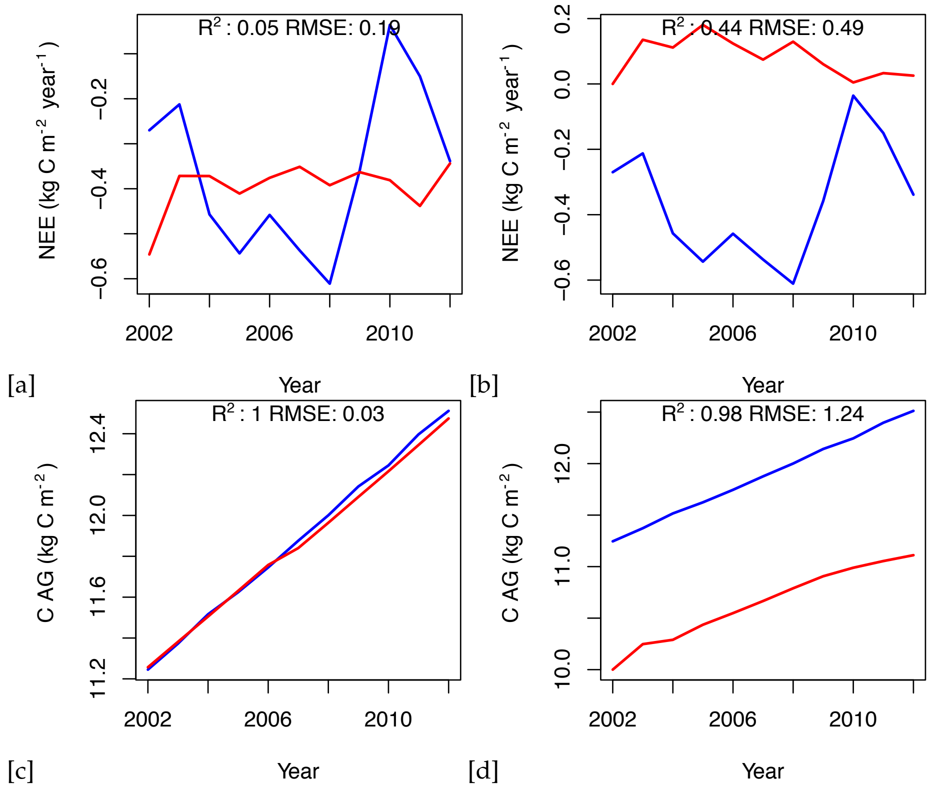

Figure 4. Simulated and observed NEE and aboveground C; observations = blue; simulations = red; a = PPA-SiBGC NEE; b = LANDIS-II NECN NEE; c = PPA-SiBGC C_{AG}; d = LANDIS-II NECN C_{AG}

An analysis of simulated species biomass and abundance also shows greater fidelity of the PPA-SiBGC model to data, as shown in Figure 5. As LANDIS-II NECN does not contain data on individual trees, species relative abundance is calculated based on the number of cohorts of each species. Two species were simulated in LANDIS-II NECN, as there are no explicit trees in the model and the number of cohorts appears to have no effect on the total biomass. Results for PPA-SiBGC indicate that species relative abundance may be improved in future studies by optimizing mortality and fecundity rates. Meanwhile, species biomass predictions output by LANDIS-II NECN were inverted from those of the observations.

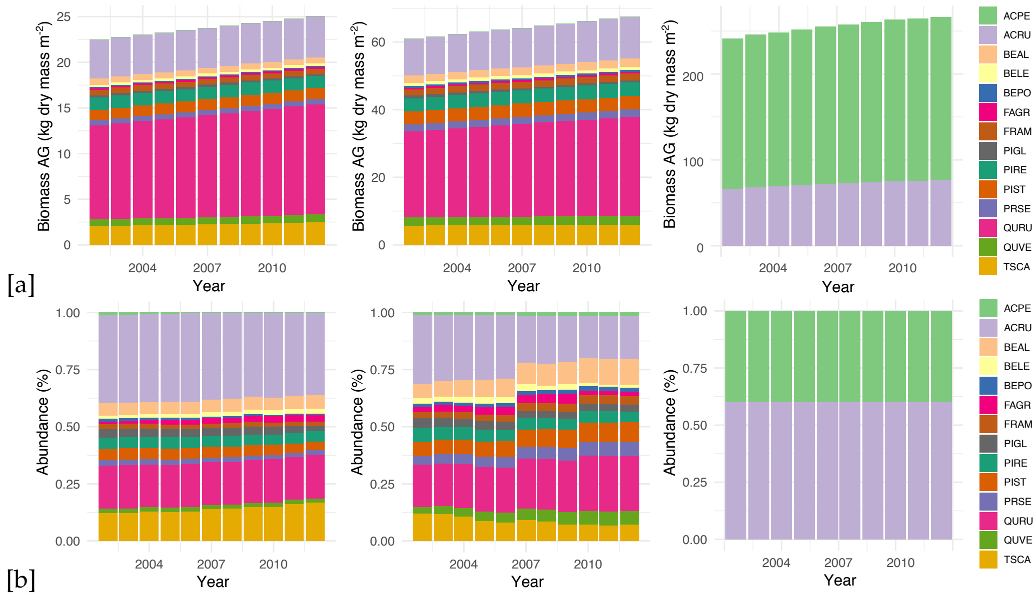

Figure 5. HF-EMS: Simulated and observed species aboveground biomass and relative abundance; a = biomass; b = abundance; left = observations, middle = PPA-SiBGC, right = LANDIS-II NECN; note that different scales are used for biomass

3.2. JERC-RD

For the JERC-RD site, both models showed stronger fidelity to data than for the HF-EMS site. Again, PPA-SiBGC showed higher R^2 values and lower RMSE and MAE values compared to LANDIS-II NECN across the range of metrics tested. Yet, the margin between models was smaller for the JERC RD site. While PPA-SiBGC demonstrated higher correlations and lower errors for most metrics tested, LANDIS-II NECN outperformed PPA-SiBGC in a few cases. This includes lower error magnitude for NEE, aboveground N, belowground biomass, SOC, and SON. However, PPA-SiBGC showed correlations equal or higher for all metrics tested, and lower errors for all other metrics. Overall results for the JERC-RD site model intercomparison are shown in Table 8.

Table 8. Model fitness for JERC-RD

	PPA-SiBGC				LANDIS-II NECN			
Metric	R^2	RMSE	MAE	ME	R^2	RMSE	MAE	ME
NEE	0.30	1.68	1.64	-1.64	0.09	0.13	0.11	-0.05
B_{AG}	0.96	1.48	1.47	1.47	0.96	9.77	9.76	-9.76
C_{AG}	0.96	1.63	1.63	-1.63	0.96	4.88	4.88	-4.88
N_{AG}	0.99	0.29	0.29	0.29	0.96	0.05	0.05	-0.05
B_{BG}	0.96	10.84	10.83	10.83	0.96	1.37	1.20	1.20
C_{BG}	0.96	5.26	5.26	-5.26	0.96	6.46	6.46	-6.46
N_{BG}	0.98	1.44	1.44	-1.44	0.96	1.60	1.60	-1.60
r_{soil}	0.19	0.78	0.71	-0.67	0.05	2.40	2.40	-2.40
ANPP	0.03	0.39	0.37	-0.37	0.03	0.48	0.46	0.25
C_{SO}	...	4.30	4.30	4.30	...	0.17	0.17	-0.17
N_{SO}	...	0.38	0.38	0.38	...	0.12	0.12	0.12
B_{Sp}	1.00	6.47	3.90	3.90	0.98	28.97	20.52	20.52
n_{Sp}	1.00	0.02	0.01	-0	1.00	0.09	0.09	-0.02
Mean	0.76	2.69	2.48	0.78	0.72	4.34	3.68	-0.25

While both models showed higher performance at the JERC-RD site, an analysis of simulated species biomass and abundance again indicates greater fidelity of the PPA-SiBGC model to data, as shown in Figure 6. While LANDIS-II NECN overpredicts the rate of longleaf pine growth, PPA-SiBGC nearly perfectly matches observed species abundance and biomass trajectories for all species present. While the correlations are high, PPA-SiBGC overpredicts the magnitude of biomass here.

Figure 6. JERC-RD: Simulated and observed species aboveground biomass and relative abundance; a = biomass; b = abundance; left = observations, middle = PPA-SiBGC, right = LANDIS-II NECN; note that different scales are used for biomass

Our results for the HF-EMS and JERC-RD site model intercomparison exercise clearly indicate strong performance for both models at both sites. Results for the JERC-RD site are particularly close between the two models. Next, we assess results related to the logistics of model deployment to new computers, users, and modeling sites.

3.3. Model Usability, Performance, and Transferability

While the two models share a similar basis in forest dynamics and biogeochemistry modeling, they differ in important practical and conceptual terms. The command-line version of the PPA-SiBGC model used in this work, version 5.0, consists of approximately 500 lines of R code and is thus readily cross-platform, including cloud providers. Meanwhile, the LANDIS-II model core and NECN succession extension are an estimated 2,000 and 0.5 million lines of code, respectively. While this version of PPA-SiBGC fuses an explicit tree canopy geometry model with empirical data on fecundity, growth, mortality, and stoichiometry, the NECN extension of LANDIS-II borrows heavily from the process-based Century model [20], similar to the MAPSS-Century-1 (MC1) model [82]. This carries important implications for model parameterization needs. While PPA-SiBGC relies on typical forest inventory data, including tree species, age/size, and densities, LANDIS-II relies on species age/size and traits in the form of vital attributes, in addition to NECN parameters. Below, we summarize our findings regarding the logistics of model deployment.

3.3.1. Model Usability

In the following section, we provide an assessment of model usability based on four criteria.

1. *Ease of installation*
   While LANDIS-II NECN requires the installation of two Windows programs, depending on the options desired, PPA-SiBGC is contained in a single R script and requires only a working R installation.

2. *Ease of parameterization*
   While both models can be difficult to parameterize for regions with little to no observational data, the simple biogeochemistry in PPA-SiBGC requires an order of magnitude fewer parameters than LANDIS-II NECN. In addition, PPA-SiBGC uses commonly available forest inventory data while NECN requires a number of parameters that may be difficult to locate.
3. *Ease of program operation*
   Both models use a command-line interface and are thus equally easy to operate. Yet, PPA-SiBGC is cross-platform and uses comma-separated-value (CSV) files for input tables, which are easier to work with than multiple tables nested within an unstructured text files. This additionally allows for simplification in designing model application programming interfaces (APIs), or model wrappers, a layer of abstraction above the models. These abstractions are important for simplifying model operation and reproducibility, and enable a number of research applications.
4. *Ease of parsing outputs*
   All PPA-SiBGC outputs are provided in CSV files in a single folder while LANDIS-II NECN generates outputs in multiple formats in multiple folders. While the PPA-SiBGC format is simpler and easier to parse, the image output formats used by LANDIS-II carry considerable benefit for spatial applications. Both models may benefit by transitioning spatiotemporal data to the NetCDF scientific file format used by most general circulation and terrestrial biosphere models.

3.3.2. Model Performance

Next, we assess model performance in terms of the speed of operation on a consumer-off-the-shelf (COTS) laptop computer with a dual-core 2.8 GHz Intel Core i7-7600U CPU and 16 GB of DDR4-2400 RAM. We focus on a single performance metric, the timing of simulations. Other aspects of model performance in the form of precision and accuracy are described in previous sections. As shown in Table 9, PPA-SiBGC was between 1,200 and 2,800% faster than LANDIS-II NECN in our timing tests. This was surprising given that PPA-SiBGC models true cohorts (i.e., individual trees) in an interpreted language while LANDIS-II models theoretical cohorts (i.e., cohorts without a physical basis) in a compiled language. The difference in speed is likely attributable to the parsimony of the PPA-SiBGC model.

Table 9. Simulation timing results

Site	Model	Duration (years)	Elapsed (sec)
HF-EMS	PPA-SiBGC	11	8.51
HF-EMS	LANDIS-II NECN	11	101.15
JERC-RD	PPA-SiBGC	5	2.25
JERC-RD	LANDIS-II NECN	5	61.51

3.3.3. Model Transferability

Here, we discuss model transferability. In this section, we assess the effort required to transfer the models to new locations, new computer systems, or new users. All three are important logistical criteria for effective model deployment.

1. *Model generalization*
   Both models appear to generalize effectively to different forested regions of the world, as both have shown strong performance in this study and others. No clear winner is evident in this regard. In terms of model realism, PPA-SiBGC has a more realistic representation of forest canopies while LANDIS-II NECN has more realistic processes, as it is a Century model variant.
2. *Availability of parameterization data*
   While LANDIS-II NECN requires substantially greater parameterization data compared to PPA-SiBGC, it may often be possible to rely on previously published parameters. Meanwhile,

the growth, mortality, and fecundity parameters used by PPA-SiBGC are easy to calculate using common field inventory data. PPA-SiBGC is simpler to transfer in this regard given the wide availability of forest inventory data.

3. *Size of the program*
   PPA-SiBGC is approximately 500 lines of R code, while LANDIS-II NECN is estimated at 0.5 million lines of C# code.
4. *Cross-platform support*
   While Linux support may soon be supported with Microsoft .NET Core, LANDIS-II NECN is written in C# and is thus limited to Microsoft Windows platforms. Meanwhile, PPA-SiBGC is written in standard R code and is fully cross-platform.
5. *Ease of training new users*
   While both models have a learning curve, the practical simplicity of PPA-SiBGC may make it easier to train new users. While LANDIS-II NECN contains more mechanistic processes and related parameters, these come at the cost of confusing new users. The model wrapper library we developed as part of this work vastly eases the operation of both models. Future studies should measure the time required for new users to effectively operate both models.

3.4. Discussion

On average, the PPA-SiBGC model outperformed LANDIS-II NECN for the sites and metrics tested, showing stronger correlations, lower error, and less bias. Despite being a parsimonious model, PPA-SiBGC contains more realistic representation of stand canopy dynamics. Meanwhile, LANDIS-II NECN contains more realistic representation of biogeochemical processes, as a simplified variant of the Century model. These differences together with the results lend support to our hypothesis that vegetation dynamics drive biogeochemical pools to a higher degree than one-dimensional processes, while the latter better capture fluxes. This is evidenced by the higher performance of PPA-SiBGC in predicting pools and LANDIS-II NECN in predicting fluxes.

Empirical coefficients for the first moment of processes (e.g., growth, mortality, and fecundity) were used to parameterize the PPA-SiBGC model, while LANDIS-II NECN required a multitude of parameters for biogeochemical processes, some of which are often treated as tuning parameters. Yet, for this validation and intercomparison exercise, fully mechanistic processes were not required; both models required a host of empirical parameters that limit their prognostic abilities in their current form. Future developments with both models should improve upon this by adopting more mechanistic processes.

Replacing the simple biogeochemistry approach of PPA-SiBGC with mechanistic processes would vastly improve the energetic and biogeochemical realism of the PPA-SiBGC model. Meanwhile, LANDIS-II NECN and other variants of the Century model may improve their structural realism by incorporating canopy representations with a physical basis. This is because Century was not designed to be a plant production model [83] and contains no physically realistic representation of trees or canopies. Currently, the forest production model of Century is based theoretically on Liebig's Law (i.e., limiting factors), employing allometric and stoichiometric relations with empirical constraints. In other words, plant production is strongly constrained by site-specific limits even though the Century model is mechanistic in other ways. Meanwhile, a lack of canopy representation strongly limits the potential number and resolution of modeled processes. In short, combining the approaches of both models may yield a more optimal solution.

In addition, our results suggest that improving the representation of forest dynamics in models may yield accurate biogeochemistry predictions even when simple allometric and stoichiometric biogeochemistry relations are used, as evidenced by the performance of PPA-SiBGC. This finding supports the current widespread focus on improving the representation of vegetation dynamics in global terrestrial biosphere models [27,28,84]. The PPA provides a uniquely efficient and tractable manner of incorporating three-dimensional canopy dynamics in global models. While many mechanistic processes may be considered mature, models of soil respiration are critical to accurate C projections and require continued development [18]. In order to achieve high levels of accuracy and precision, given the recent success of aboveground model approximations, next-generation models may require a similar breakthrough in belowground processes.

Future studies should expand upon the PPA with a first-principles representation of energetic and biogeochemical above- and below-ground processes in a modern component-based software framework. This work should fuse the new state-of-the-art forest biogeochemistry model with a model wrapper API written in R or Python, in order to expand native model functions to include sampling from parameter probability distributions, Monte Carlo methods, machine-learning model emulation, robust loss functions, and optimization. This would combine a high-performance forest model written in a compiled language with a user-friendly interface in an interpreted language.

3.5. Limitations

This study, similar to other forest modeling studies, was limited by the availability of observational data. The lack of temporal depth in this data poses substantial challenges in modeling the long-term effects of forest succession, as these processes can operate on a century timescale or longer. However, assessing succession predictions was not the aim of this study, as we instead focus on near-term validation of forest models using field measurements and EC flux tower data. Another limitation is that these methods may be challenging to implement for sites that are less well-characterized, particularly in the absence of EC flux tower data and/or tree species parameters. A combination of tower-based and remote sensing observations may help overcome this challenge in the coming years with advances in machine learning.

4. Conclusions

In conclusion, the PPA-SiBGC and LANDIS-II NECN models represent vegetation dynamics previously absent in modeling studies at these sites. These include, "...long-term increases in tree biomass, successional change in forest composition, and disturbance events, processes not well represented in current models," which drive interannual variation in NEE [40]. While the timescale of our simulations were decidedly short-term due to data limitations, both models showed good performance. While PPA-SiBGC showed stronger performance across the range of metrics tested, including the logistics of model deployment, LANDIS-II NECN also performed well across the metrics tested. Further studies are needed to compare more aspects of these and other models based on an array of performance criteria.

Ultimately, we hope that this study serves as the foundation for future forest ecosystem model intercomparisons for the North American continent, similar in spirit to the former TDE Ecosystem Model Intercomparison project [24]. This may help create the impetus for a Global Forest Model Intercomparison Project (ForestMIP) together with modeling groups on other continents. The aims of this research were not to determine which model is 'best' for prognosis at two locations, but to improve the capabilities of existing models across a range of locations in order to advance earth system models. In this regard, there are beneficial aspects to both modeling approaches and the trade-offs presented largely depend on the desired application. Counter to the classical modeling trade-off of Levins [21], improvements in precision and generality resulted from realism.

Supplementary Materials: Parameter tables for both models and sites are provided in Appendix 4. All model, parameter, script files used in this model intercomparison exercise are available for download at the following public GitHub repository:

https://github.com/adam-erickson/ecosystem-model-comparison

The repository provides tables containing parameter values and climate drivers used in the PPA-SiBGC and LANDIS-II NECN model simulations for the two model intercomparison sites. Tree species codes are adopted from the USDA PLANTS database, accessible at the following URL:

https://plants.sc.egov.usda.gov

Scripts provided include a simple object-oriented forest biogeochemistry model wrapper library implemented in the R language [79]. The model wrapper library includes a number of features for simplifying the operation of this class of models, including functions for cleaning up and parsing model outputs into memory in a common format for comparison. Importantly, the wrapper library enables full reproducibility of results through the *hf_ems.r* and *jerc_rd.r* scripts. Using these scripts with the object-oriented *classes.r* model wrapper, it is possible to load pre-computed model results and calculate all intercomparison metrics for verification. The directory structure of the repository is shown in Figure 7.

```
ecosystem-model-comparison
├── figures
├── models
│   ├── landis_2
│   │   ├── hf_ems
│   │   │   ├── extensions
│   │   │   │   └── succession
│   │   │   │       └── necn
│   │   │   │           ├── climate
│   │   │   │           └── maps
│   │   │   └── outputs
│   │   │       └── succession
│   │   │           └── necn
│   │   │               ├── logs
│   │   │               └── metadata
│   │   └── jerc_rd
│   │       ├── extensions
│   │       │   └── succession
│   │       │       └── necn
│   │       │           ├── climate
│   │       │           └── maps
│   │       └── outputs
│   │           └── succession
│   │               └── necn
│   │                   ├── logs
│   │                   └── metadata
│   └── ppa_bgc
│       ├── hf_ems
│       │   ├── lut
│       │   └── outputs
│       └── jerc_rd
│           ├── lut
│           └── outputs
└── scripts
```

Figure 7. Directory structure of the GitHub repository

Author Contributions: Individual contributions provided to complete this work include the following: conceptualization, N.S.; methodology, A.E. and N.S.; software, A.E.; validation, A.E.; formal analysis, A.E.; investigation, A.E.; resources, N.S.; data curation, A.E.; writing—original draft preparation, A.E.; writing—review and editing, A.E. and N.S.; visualization, A.E.; supervision, N.S.; project administration, N.S.; funding acquisition, N.S.

Funding: This research was funded by United States Army Corps of Engineers (USACE) contract number W912HQ-18-C-0007.

Acknowledgments: We would like to thank U.S. Department of Defense, Army Corps of Engineers, and the Environmental Security Technology Certification Program (ESTCP) for providing support necessary to conduct this work. We also thank Harvard University and Jones Ecological Research Center for kindly providing data to conduct the analyses. We would further like to thank those that provided guidance on parameterization of the LANDIS-II model. We thank Drs. Louise Loudermilk of USDA Forest Service and Steven Flanagan of Tall Timbers Research Station for providing guidance on parameterization for the Red Dirt flux tower site at JERC, and Dr. Matthew Duveneck of New England Conservatory for providing guidance on parameterization for the

HF-EMS EC flux tower site at Harvard Forest. We also acknowledge Drs. Melissa Lucash and Robert Scheller, who provided comments. Last, we would like to thank Drs. Bradley Case, Hannah Buckley, Audrey Barket-Plotkin, David Orwig, Aaron Ellison and Zachary Robbins for providing some of the crown allometry parameters for Harvard Forest.

Conflicts of Interest: The authors declare no conflict of interest. The funders had no role in the design of the study; in the collection, analyses, or interpretation of data; in the writing of the manuscript, or in the decision to publish the results.

Abbreviations

The following abbreviations are used in this manuscript:

ANPP	Aboveground net primary production
API	Application programming interface
BGC	Biogeochemistry
COST	Cooperation in Science and Technology
CPU	Central processing unit
CSV	Comma-separated values
DoD	Department of Defense
EC	Eddy covariance
ED	Ecosystem Demography model
EMS	Environmental Measurement Station
FVS	Forest Vegetation Simulator
GPGPU	General-purpose graphics processing unit
HF	Harvard Forest
IBIS2	Integrated Biosphere Simulator 2
JERC	Jones Ecological Research Center
L-systems	Lindenmayer systems
LANDIS-II	Landscape Disturbance and Succession model 2
LM3	Land Model 3
LPJ-GUESS	Lund-Potsdam-Jena General Ecosystem Simulator
MAE	Mean absolute error
MC1	MAPSS-Century-1 model
NECN	Net Ecosystem Carbon and Nitrogen model
NEE	Net ecosystem exchange
NSE	Nash-Sutcliffe efficiency
PPA	Perfect Plasticity Approximation model
ProFoUnd	Towards robust projections of European forests under climate change
RAM	Random access memory
RD	Red Dirt
RMSE	Root mean squared error
SAS	Size- and age-structured equations
SOC	Soil organic carbon
SON	Soil organic nitrogen
TDE	Throughfall Displacement Experiment

References

1. Vuokila, Y. Functions for variable density yield tables of pine based on temporary sample plots. Technical report, Finnish Forest Research Institute, Helsinki, Finland, 1965.
2. Usher, M.B. A Matrix Approach to the Management of Renewable Resources, with Special Reference to Selection Forests. *Journal of Applied Ecology* **1966**, *3*, 355–367. doi:10.2307/2401258.
3. Stage, A.R. Prognosis model for stand development. Res. Pap. INT-RP-137. Technical report, U.S. Dept. of Agriculture, Forest Service, Intermountain Forest and Range Experiment Station, Ogden, Utah, USA, 1973.
4. Crookston, N.L.; Dixon, G.E. The forest vegetation simulator: A review of its structure, content, and applications. *Computers and Electronics in Agriculture* **2005**, *49*, 60–80. doi:https://doi.org/10.1016/j.compag.2005.02.003.

5. Systems, N.; Products, W.; Bugmann, H.; Yan, X.; Sykes, M.; Martin, P.; Lindner, M.; Desanker, P.; Cumming, S. A comparison of forest gap models: Model structure and behaviour. *Climatic Change* **1996**, *34*, 289–313. doi:10.1007/BF00224640.
6. Keane, R.E.; Cary, G.J.; Davies, I.D.; Flannigan, M.D.; Gardner, R.H.; Lavorel, S.; Lenihan, J.M.; Li, C.; Rupp, T. A classification of landscape fire succession models: spatial simulations of fire and vegetation dynamics. *Ecological Modelling* **2004**, *179*, 3 – 27. doi:https://doi.org/10.1016/j.ecolmodel.2004.03.015.
7. Mladenoff, D.J. LANDIS and forest landscape models. *Ecological Modelling* **2004**, *180*, 7–19. doi:10.1016/j.ecolmodel.2004.03.016.
8. He, H.S. Forest landscape models: Definitions, characterization, and classification. *Forest Ecology and Management* **2008**, *254*, 484–498. doi:10.1016/j.foreco.2007.08.022.
9. Xi, W.; Coulson, R.N.; Birt, A.G.; Shang, Z.B.; Waldron, J.D.; Lafon, C.W.; Cairns, D.M.; Tchakerian, M.D.; Klepzig, K.D. Review of forest landscape models: Types, methods, development and applications. *Acta Ecologica Sinica* **2009**, *29*, 69–78. doi:10.1016/j.chnaes.2009.01.001.
10. Shifley, S.R.; He, H.S.; Lischke, H.; Wang, W.J.; Jin, W.; Gustafson, E.J.; Thompson, J.R.; Thompson, F.R.; Dijak, W.D.; Yang, J. The past and future of modeling forest dynamics: from growth and yield curves to forest landscape models. *Landscape Ecology* **2017**, *32*, 1307–1325. doi:10.1007/s10980-017-0540-9.
11. Sellers, P.J.; Mintz, Y.; Sud, Y.C.; Dalcher, A. A Simple Biosphere Model (SIB) for Use within General Circulation Models. *Journal of the Atmospheric Sciences* **1986**, *43*, 505–531. doi:10.1175/1520-0469(1986)043<0505:ASBMFU>2.0.CO;2.
12. Fisher, J.B.; Huntzinger, D.N.; Schwalm, C.R.; Sitch, S. Modeling the Terrestrial Biosphere. *Annual Review of Environment and Resources* **2014**, *39*, 91–123. doi:10.1146/annurev-environ-012913-093456.
13. Fisher, R.A.; Koven, C.D.; Anderegg, W.R.L.; Christoffersen, B.O.; Dietze, M.C.; Farrior, C.E.; Holm, J.A.; Hurtt, G.C.; Knox, R.G.; Lawrence, P.J.; Lichstein, J.W.; Longo, M.; Matheny, A.M.; Medvigy, D.; Muller-Landau, H.C.; Powell, T.L.; Serbin, S.P.; Sato, H.; Shuman, J.K.; Smith, B.; Trugman, A.T.; Viskari, T.; Verbeeck, H.; Weng, E.; Xu, C.; Xu, X.; Zhang, T.; Moorcroft, P.R. Vegetation demographics in Earth System Models: A review of progress and priorities. *Global Change Biology* **2018**, *24*, 35–54. doi:10.1111/gcb.13910.
14. Duursma, R.A.; Medlyn, B.E. MAESPA: a model to study interactions between water limitation, environmental drivers and vegetation function at tree and stand levels, with an example application to CO2 x drought interactions. *Geoscientific Model Development* **2012**, *5*, 919–940. doi:10.5194/gmd-5-919-2012.
15. Liénard, J.; Strigul, N. An individual-based forest model links canopy dynamics and shade tolerances along a soil moisture gradient. *Royal Society Open Science* **2016**, *3*.
16. Landsberg, J.J.; Waring, R.H. A generalised model of forest productivity using simplified concepts of radiation-use efficiency, carbon balance and partitioning. *Forest Ecology and Management* **1997**, *95*, 209–228. doi:http://dx.doi.org/10.1016/S0378-1127(97)00026-1.
17. Farquhar, G.D.; von Caemmerer, S.; Berry, J.A. A biochemical model of photosynthetic CO2 assimilation in leaves of C3 species. *Planta* **1980**, *149*, 78–90. doi:10.1007/BF00386231.
18. Sulman, B.N.; Moore, J.A.M.; Abramoff, R.; Averill, C.; Kivlin, S.; Georgiou, K.; Sridhar, B.; Hartman, M.D.; Wang, G.; Wieder, W.R.; Bradford, M.A.; Luo, Y.; Mayes, M.A.; Morrison, E.; Riley, W.J.; Salazar, A.; Schimel, J.P.; Tang, J.; Classen, A.T. Multiple models and experiments underscore large uncertainty in soil carbon dynamics. *Biogeochemistry* **2018**, *141*, 109–123. doi:10.1007/s10533-018-0509-z.
19. Parton, W. Simulation of organic matter formation and mineralization in semi-arid agroecosystems. *Nutrient Cycling in Agricultural Ecosystems Specl. Publ. 23* **1983**, pp. 533–550.
20. Parton, W.J.; Schimel, D.S.; Cole, C.V.; Ojima, D.S. Analysis of Factors Controlling Soil Organic Matter Levels in Great Plains Grasslands1. *Soil Science Society of America Journal* **1987**, *51*, 1173–1179. doi:10.2136/sssaj1987.03615995005100050015x.
21. Levins, R. The Strategy of Model Building in Population Biology. *American Scientist* **1966**, *54*, 421–431.
22. Warszawski, L.; Frieler, K.; Huber, V.; Piontek, F.; Serdeczny, O.; Schewe, J. The Inter-Sectoral Impact Model Intercomparison Project (ISI–MIP): Project framework. *Proceedings of the National Academy of Sciences* **2014**, *111*, 3228–3232, [http://www.pnas.org/content/111/9/3228.full.pdf]. doi:10.1073/pnas.1312330110.
23. Lischke, H.; Speich, M.; Schmatz, D.; Vacchiano, G.; Mairota, P.; Leronni, V.; Schuler, L.; Bugmann, H.; Bruna, J.; Thom, D.; Seidl, R.; Reineking, B. CoFoLaMo: Comparing forest landscape model simulations under different climate, interaction- and land use scenarios. EGU General Assembly Conference Abstracts, 2016, Vol. 18, *EGU General Assembly Conference Abstracts*, pp. EPSC2016–13867.

24. Hanson, P.J.; Amthor, J.S.; Wullschleger, S.D.; Wilson, K.B.; Grant, R.F.; Hartley, A.; Hui, D.; Hunt, E.R.; Johnson, D.W.; Kimball, J.S.; King, A.W.; Luo, Y.; McNulty, S.G.; Sun, G.; Thornton, P.E.; Wang, S.; Williams, M.; Baldocchi, D.D.; Cushman, R.M. Oak Forest Carbon and Water Simulations: Model Intercomparisons and Evaluations against Independent Data. *Ecological Monographs* **2004**, *74*, 443–489.
25. Kimmins, J.; Mailly, D.; Seely, B. Modelling forest ecosystem net primary production: the hybrid simulation approach used in forecast. *Ecological Modelling* **1999**, *122*, 195–224. doi:10.1016/S0304-3800(99)00138-6.
26. Kimmins, H.; Blanco, J.A.; Seely, B.; Welham, C.; Scoullar, K. *Forecasting Forest Futures: A Hybrid Modelling Approach to the Assessment of Sustainability of Forest Ecosystems and Their Values*; Taylor & Francis Group, 2010; p. 296.
27. Fisher, R.; McDowell, N.; Purves, D.; Moorcroft, P.; Sitch, S.; Cox, P.; Huntingford, C.; Meir, P.; Ian Woodward, F. Assessing uncertainties in a second-generation dynamic vegetation model caused by ecological scale limitations. *New Phytologist* **2010**, *187*, 666–681. doi:10.1111/j.1469-8137.2010.03340.x.
28. Ahlström, A.; Xia, J.; Arneth, A.; Luo, Y.; Smith, B. Importance of vegetation dynamics for future terrestrial carbon cycling. *Environmental Research Letters* **2015**, *10*, 054019.
29. Sitch, S.; Smith, B.; Prentice, I.C.; Arneth, A.; Bondeau, A.; Cramer, W.; Kaplan, J.O.; Levis, S.; Lucht, W.; Sykes, M.T.; Thonicke, K.; Venevsky, S. Evaluation of ecosystem dynamics, plant geography and terrestrial carbon cycling in the LPJ dynamic global vegetation model. *Global Change Biology* **2003**, *9*, 161–185. doi:10.1046/j.1365-2486.2003.00569.x.
30. Moorcroft, P.R.; Hurtt, G.C.; Pacala, S.W. A method for scaling vegetation dynamics: The ecosystem demography model (ED). *Ecological Monographs* **2001**, *71*, 557–586. doi:10.1890/0012-9615(2001)071[0557:AMFSVD]2.0.CO;2.
31. Medvigy, D.; Wofsy, S.C.; Munger, J.W.; Hollinger, D.Y.; Moorcroft, P.R. Mechanistic scaling of ecosystem function and dynamics in space and time: Ecosystem Demography model version 2. *Journal of Geophysical Research: Biogeosciences* **2009**, *114*. doi:10.1029/2008JG000812.
32. Weng, E.S.; Malyshev, S.; Lichstein, J.W.; Farrior, C.E.; Dybzinski, R.; Zhang, T.; Shevliakova, E.; Pacala, S.W. Scaling from individual trees to forests in an Earth system modeling framework using a mathematically tractable model of height-structured competition. *Biogeosciences* **2015**, *12*, 2655–2694. doi:10.5194/bg-12-2655-2015.
33. Strigul, N.; Pristinski, D.; Purves, D.; Dushoff, J.; Pacala, S. Scaling from trees to forests: tractable macroscopic equations for forest dynamics. *Ecological Monographs* **2008**, *78*, 523–545, [http://www.esajournals.org/doi/pdf/10.1890/08-0082.1]. doi:10.1890/08-0082.1.
34. Purves, D.W.; Lichstein, J.W.; Strigul, N.; Pacala, S.W. Predicting and understanding forest dynamics using a simple tractable model. *Proceedings of the National Academy of Sciences* **2008**, *105*, 17018–17022, [http://www.pnas.org/content/105/44/17018.full.pdf]. doi:10.1073/pnas.0807754105.
35. Davis, A.V. Testing LANDIS-II to stochastically model spatially abstract vegetation trends in the contiguous United States. Thesis, University of Southern California, 2013.
36. Strigul, N. Individual-based models and scaling methods for ecological forestry: implications of tree phenotypic plasticity. In *Sustainable Forest Management*; Garcia, J.; Casero, J., Eds.; InTech: Rijeka, Croatia, 2012; pp. 359–384. http://dx.doi.org/10.5772/29590.
37. Liénard, J.; Strigul, N. An individual-based forest model links canopy dynamics and shade tolerances along a soil moisture gradient. *Royal Society Open Science* **2016**, *3*, 150589.
38. Seidl, R.; Rammer, W.; Scheller, R.M.; Spies, T.a. An individual-based process model to simulate landscape-scale forest ecosystem dynamics. *Ecological Modelling* **2012**, *231*, 87–100. doi:10.1016/j.ecolmodel.2012.02.015.
39. Giasson, M.A.; Ellison, A.M.; Bowden, R.D.; Crill, P.M.; Davidson, E.A.; Drake, J.E.; Frey, S.D.; Hadley, J.L.; Lavine, M.; Melillo, J.M.; Munger, J.W.; Nadelhoffer, K.J.; Nicoll, L.; Ollinger, S.V.; Savage, K.E.; Steudler, P.A.; Tang, J.; Varner, R.K.; Wofsy, S.C.; Foster, D.R.; Finzi, A.C. Soil respiration in a northeastern US temperate forest: a 22-year synthesis. *Ecosphere* **2013**, *4*, art140, [https://esajournals.onlinelibrary.wiley.com/doi/pdf/10.1890/ES13.00183.1]. doi:10.1890/ES13.00183.1.
40. Urbanski, S.; Barford, C.; Wofsy, S.; Kucharik, C.; Pyle, E.; Budney, J.; McKain, K.; Fitzjarrald, D.; Czikowsky, M.; Munger, J.W. Factors controlling CO2 exchange on timescales from hourly to decadal at Harvard Forest. *Journal of Geophysical Research: Biogeosciences* **2007**, *112*, [https://agupubs.onlinelibrary.wiley.com/doi/pdf/10.1029/2006JG000293]. doi:10.1029/2006JG000293.

41. Scheller, R.M.; Domingo, J.B.; Sturtevant, B.R.; Williams, J.S.; Rudy, A.; Gustafson, E.J.; Mladenoff, D.J. Design, development, and application of LANDIS-II, a spatial landscape simulation model with flexible temporal and spatial resolution. *Ecological Modelling* **2007**, *201*, 409–419. doi:10.1016/j.ecolmodel.2006.10.009.
42. Scheller, R.M.; Hua, D.; Bolstad, P.V.; Birdsey, R.A.; Mladenoff, D.J. The effects of forest harvest intensity in combination with wind disturbance on carbon dynamics in Lake States Mesic Forests. *Ecological Modelling* **2011**, *222*, 144–153. doi:https://doi.org/10.1016/j.ecolmodel.2010.09.009.
43. Whelan, A.; Mitchell, R.; Staudhammer, C.; Starr, G. Cyclic Occurrence of Fire and Its Role in Carbon Dynamics along an Edaphic Moisture Gradient in Longleaf Pine Ecosystems. *PLOS ONE* **2013**, *8*, 1–15. doi:10.1371/journal.pone.0054045.
44. Wiesner, S.; Staudhammer, C.L.; Loescher, H.W.; Baron-Lopez, A.; Boring, L.R.; Mitchell, R.J.; Starr, G. Interactions Among Abiotic Drivers, Disturbance and Gross Ecosystem Carbon Exchange on Soil Respiration from Subtropical Pine Savannas. *Ecosystems* **2018**. doi:10.1007/s10021-018-0246-0.
45. Starr, G.; Staudhammer, C.L.; Loescher, H.W.; Mitchell, R.; Whelan, A.; Hiers, J.K.; O'Brien, J.J. Time series analysis of forest carbon dynamics: recovery of Pinus palustris physiology following a prescribed fire. *New Forests* **2015**, *46*, 63–90. doi:10.1007/s11056-014-9447-3.
46. Hawkins, D.M. The Problem of Overfitting. *Journal of Chemical Information and Computer Sciences* **2004**, *44*, 1–12. doi:10.1021/ci0342472.
47. Mladenoff, D.J.; Host, G.E.; Boeder, J.; Crow, T.R. LANDIS: a spatial model of forest landscape disturbance, succession, and management. Second International Conference on Integrating Modelling and GIS, 1993.
48. Mladenoff, D.J.; He, H.S. Design, behavior and application of LANDIS, an object-oriented model of forest landscape disturbance and succession. In *Spatial Modeling of Forest Landscape Change: Approaches and Applications*; Cambridge University Press: Cambridge, UK, 1999; pp. 125–162.
49. He, H.S.; Mladenoff, D.J.; Boeder, J. An object-oriented forest landscape model and its representation of tree species. *Ecological Modelling* **1999**, *119*, 1–19. doi:10.1016/S0304-3800(99)00041-1.
50. Wang, W.J.; He, H.S.; Fraser, J.S.; Thompson, F.R.; Shifley, S.R.; Spetich, M.A. LANDIS PRO: a landscape model that predicts forest composition and structure changes at regional scales. *Ecography* **2014**, *37*, 225–229, [https://onlinelibrary.wiley.com/doi/pdf/10.1111/j.1600-0587.2013.00495.x]. doi:10.1111/j.1600-0587.2013.00495.x.
51. Pennanen, J.; Kuuluvainen, T. A spatial simulation approach to natural forest landscape dynamics in boreal Fennoscandia. *Forest Ecology and Management* **2002**, *164*, 157–175. doi:https://doi.org/10.1016/S0378-1127(01)00608-9.
52. Pennanen, J.; Greene, D.F.; Fortin, M.J.; Messier, C. Spatially explicit simulation of long-term boreal forest landscape dynamics: incorporating quantitative stand attributes. *Ecological Modelling* **2004**, *180*, 195–209. Modelling disturbance and succession in forest landscapes using LANDIS, doi:https://doi.org/10.1016/j.ecolmodel.2004.02.023.
53. Roberts, D.W.; Betz, D.W. Simulating landscape vegetation dynamics of Bryce Canyon National Park with the vital attributes/fuzzy systems model VAFS/LANDSIM. In *Spatial Modeling of Forest Landscape Change: Approaches and Applications*; Cambridge University Press: Cambridge, UK, 1999; pp. 99–123.
54. Von Neumann, J.; Burks, A.W.; others. Theory of self-reproducing automata. *IEEE Transactions on Neural Networks* **1966**, *5*, 3–14.
55. Noble, I.; Slatyer, R. The use of vital attributes to predict successional changes in plant communities subject to recurrent disturbances. *Succession* **1980**.
56. Rothermel, Richard C. A mathematical model for predicting fire spread in wildland fuels. Res. Pap. INT-115. Technical report, U.S. Department of Agriculture, Intermountain Forest and Range Experiment Station, Ogden, Utah, USA, 1972.
57. ISO. *ISO/IEC 14882:1998: Programming languages — C++*; pub-ISO: pub-ISO:adr, 1998; p. 732. Available in electronic form for online purchase at `http://webstore.ansi.org/` and `http://www.cssinfo.com/`.
58. Manabe, S. Climate and the Ocean Circulation. *Monthly Weather Review* **1969**, *97*, 739–774. doi:10.1175/1520-0493(1969)097<0739:CATOC>2.3.CO;2.
59. Thompson, J.R.; Foster, D.R.; Scheller, R.; Kittredge, D. The influence of land use and climate change on forest biomass and composition in Massachusetts, USA. *Ecological applications : a publication of the Ecological Society of America* **2011**, *21*, 2425–44.

60. Duveneck, M.J.; Thompson, J.R.; Gustafson, E.J.; Liang, Y.; de Bruijn, A.M.G. Recovery dynamics and climate change effects to future New England forests. *Landscape Ecology* **2017**, *32*, 1385–1397. doi:10.1007/s10980-016-0415-5.
61. Duveneck, M.J.; Scheller, R.M.; White, M.A.; Handler, S.D.; Ravenscroft, C. Climate change effects on northern Great Lake (USA) forests: A case for preserving diversity. *Ecosphere* **2014**, *5*, art23. doi:10.1890/ES13-00370.1.
62. Lucash, M.S.; Scheller, R.M.; J. Gustafson, E.; R. Sturtevant, B. Spatial resilience of forested landscapes under climate change and management. *Landscape Ecology* **2017**, *32*, 953–969. doi:10.1007/s10980-017-0501-3.
63. Pacala, S.W.; Canham, C.D.; Jr., J.A.S. Forest models defined by field measurements: I. The design of a northeastern forest simulator. *Canadian Journal of Forest Research* **1993**, *23*, 1980–1988. doi:10.1139/x93-249.
64. Ribbens, E.; Silander, J.A.; Pacala, S.W. Seedling recruitment in forests: calibrating models to predict patterns of tree seedling dispersion. *Ecology* **1994**, *75*, 1794–1806. doi:10.2307/1939638.
65. Hurtt, G.C.; Moorcroft, P.R.; And, S.W.P.; Levin, S.A. Terrestrial models and global change: challenges for the future. *Global Change Biology* **1998**, *4*, 581–590, [https://onlinelibrary.wiley.com/doi/pdf/10.1046/j.1365-2486.1998.t01-1-00203.x]. doi:10.1046/j.1365-2486.1998.t01-1-00203.x.
66. Robbins, Z.; Scheller, R.; Case, B.; Strigul, N. The parameterization of PPA formulas using a SORTIE-ND Model for Harvard Forest. Abstracts of the AMS Spring Western Sectional Meeting, 2018. http://www.ams.org/amsmtgs/2248_abstracts/1137-92-206.pdf.
67. García, O. Can plasticity make spatial structure irrelevant in individual-tree models? *Forest Ecosystems* **2014**, *1*, 16.
68. Lee, M.J.; García, O. Plasticity and extrapolation in modeling mixed-species stands. *Forest Science* **2016**, *62*, 1–8.
69. Raich, J.W.; Potter, C.S.; Bhagawati, D. Interannual variability in global soil respiration, 1980–94. *Global Change Biology* **2002**, *8*, 800–812, [https://onlinelibrary.wiley.com/doi/pdf/10.1046/j.1365-2486.2002.00511.x]. doi:10.1046/j.1365-2486.2002.00511.x.
70. Domke, G.M.; Perry, C.H.; Walters, B.F.; Nave, L.E.; Woodall, C.W.; Swanston, C.W. Toward inventory-based estimates of soil organic carbon in forests of the United States. *Ecological Applications* **2017**, *27*, 1223–1235, [https://esajournals.onlinelibrary.wiley.com/doi/pdf/10.1002/eap.1516]. doi:10.1002/eap.1516.
71. Canham, C.D.; Coates, K.D.; Bartemucci, P.; Quaglia, S. Measurement and modeling of spatially explicit variation in light transmission through interior cedar-hemlock forests of British Columbia. *Canadian Journal of Forest Research* **1999**, *29*, 1775–1783, [https://doi.org/10.1139/x99-151]. doi:10.1139/x99-151.
72. Case, B.S.; Buckley, H.L.; Barker-Plotkin, A.A.; Orwig, D.A.; Ellison, A.M. When a foundation crumbles: forecasting forest dynamics following the decline of the foundation species Tsuga canadensis. *Ecosphere* **2017**, *8*, e01893, [https://esajournals.onlinelibrary.wiley.com/doi/pdf/10.1002/ecs2.1893]. doi:10.1002/ecs2.1893.
73. Chojnacky, D.C.; Heath, L.S.; Jenkins, J.C. Updated generalized biomass equations for North American tree species. *Forestry: An International Journal of Forest Research* **2014**, *87*, 129–151, [/oup/backfile/content$_{p}ublic/journal/forestry/87/1/10.1093/forestry/cpt053/2/cpt053.pdf$]. doi:10.1093/forestry/cpt053.
74. Barford, C.C.; Wofsy, S.C.; Goulden, M.L.; Munger, J.W.; Pyle, E.H.; Urbanski, S.P.; Hutyra, L.; Saleska, S.R.; Fitzjarrald, D.; Moore, K. Factors Controlling Long- and Short-Term Sequestration of Atmospheric CO2 in a Mid-latitude Forest. *Science* **2001**, *294*, 1688–1691, [http://science.sciencemag.org/content/294/5547/1688.full.pdf]. doi:10.1126/science.1062962.
75. HENDRICKS, J.J.; HENDRICK, R.L.; WILSON, C.A.; MITCHELL, R.J.; PECOT, S.D.; GUO, D. Assessing the patterns and controls of fine root dynamics: an empirical test and methodological review. *Journal of Ecology* **2005**, *94*, 40–57, [https://besjournals.onlinelibrary.wiley.com/doi/pdf/10.1111/j.1365-2745.2005.01067.x]. doi:10.1111/j.1365-2745.2005.01067.x.
76. Drew, M.B.; Kirkman, L.K.; Angus K. Gholson, J. The Vascular Flora of Ichauway, Baker County, Georgia: A Remnant Longleaf Pine/Wiregrass Ecosystem. *Castanea* **1998**, *63*, 1–24.

77. Goebel, P.C.; Hix, D.M. Changes in the composition and structure of mixed-oak, second-growth forest ecosystems during the understory reinitiation stage of stand development. *Ecoscience* **1997**, *4*, 327–339, [https://doi.org/10.1080/11956860.1997.11682412]. doi:10.1080/11956860.1997.11682412.
78. Mitchell, R.J.; Kirkman, L.K.; Pecot, S.D.; Wilson, C.A.; Palik, B.J.; Boring, L.R. Patterns and controls of ecosystem function in longleaf pine - wiregrass savannas. I. Aboveground net primary productivity. *Canadian Journal of Forest Research* **1999**, *29*, 743–751, [https://doi.org/10.1139/x99-051]. doi:10.1139/x99-051.
79. R Core Team. *R: A Language and Environment for Statistical Computing*. R Foundation for Statistical Computing, Vienna, Austria, 2018.
80. Krause, P.; Boyle, D.P.; Bäse, F. Comparison of different efficiency criteria for hydrological model assessment. *Advances in Geosciences* **2005**, *5*, 89–97. doi:10.5194/adgeo-5-89-2005.
81. Nash, J.; Sutcliffe, J. River flow forecasting through conceptual models part I — A discussion of principles. *Journal of Hydrology* **1970**, *10*, 282–290. doi:https://doi.org/10.1016/0022-1694(70)90255-6.
82. Bachelet, D.; Lenihan, J.M.; Daly, C.; Neilson, R.P.; Ojima, D.S.; Parton, W.J. MC1: a dynamic vegetation model for estimating the distribution of vegetation and associated ecosystem fluxes of carbon, nutrients, and water. *Pacific Northwest Station General Technical Report PNW-GTR-508* **2001**.
83. Metherell, A.K.; Harding, L.A.; Vernon, C.C.; J, P.W. CENTURY Soil Organic Matter Model Environment, Agroecosystem Version 4.0, Technical Report No. 4. Technical report, USDA-ARS, Great Plains System Research Unit, Fort Collins, CO, USA, 1996.
84. Friend, A.D.; Lucht, W.; Rademacher, T.T.; Keribin, R.; Betts, R.; Cadule, P.; Ciais, P.; Clark, D.B.; Dankers, R.; Falloon, P.D.; Ito, A.; Kahana, R.; Kleidon, A.; Lomas, M.R.; Nishina, K.; Ostberg, S.; Pavlick, R.; Peylin, P.; Schaphoff, S.; Vuichard, N.; Warszawski, L.; Wiltshire, A.; Woodward, F.I. Carbon residence time dominates uncertainty in terrestrial vegetation responses to future climate and atmospheric CO2. *Proceedings of the National Academy of Sciences* **2014**, *111*, 3280–3285. doi:10.1073/pnas.1222477110.

Appendix A. Eddy covariance flux tower measurements

Appendix A.1. HF-EMS EC Flux Tower

Recent historical mean daily fluxes of temperature ($^{\circ}\,C$), ecosystem respiration ($\mu mol\ CO_2\ m^{-2}$), and NEE ($\mu mol\ C\ m^{-2}$) for the HF-EMS tower are shown in Figure A1.

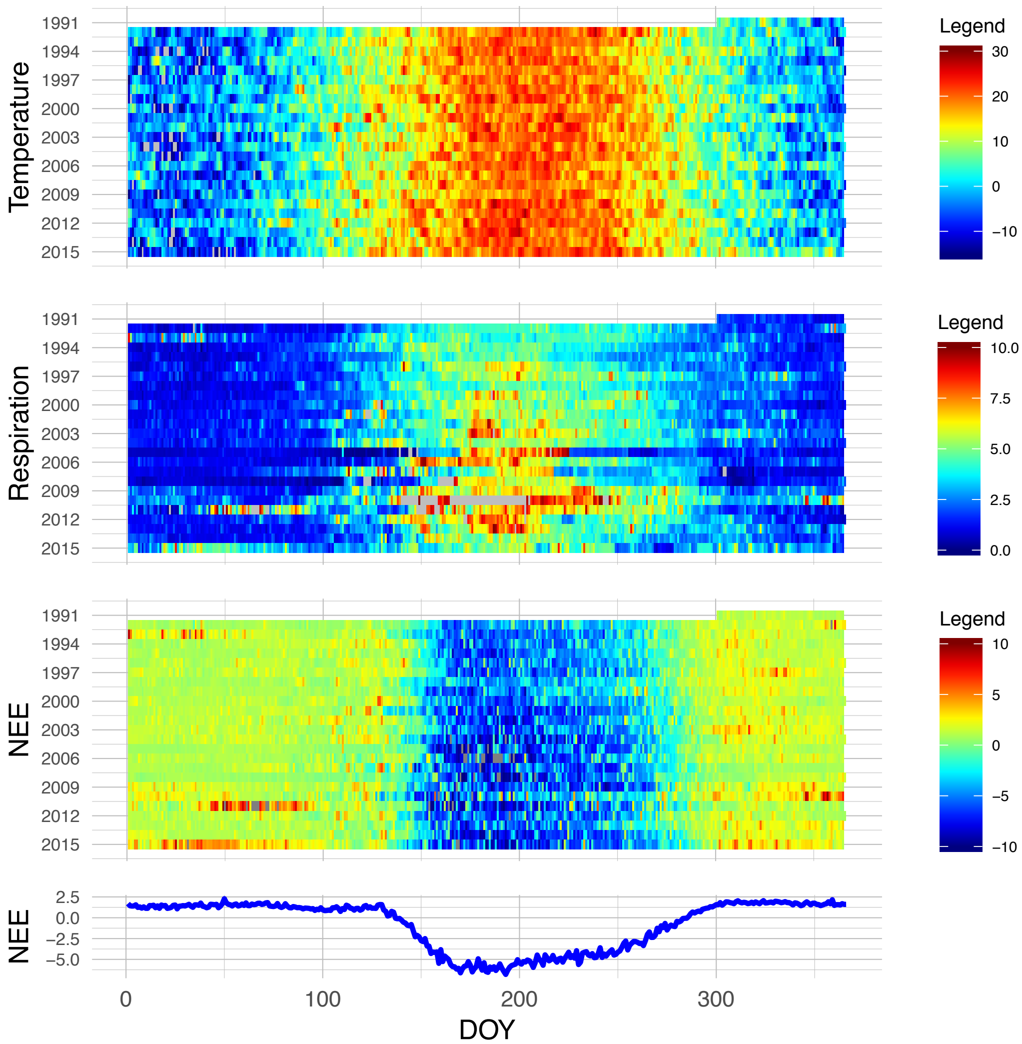

Figure A1. HF-EMS tower daily averages

Patterns in daytime and nighttime NEE are shown in Figure A2. This was calculated by taking daily mean NEE values for three-hour windows surrounding noon and midnight, respectively (1100-1300 and 2300-0100 hours). These patterns are important to diagnose, as they demonstrate responses to a gradient of light and temperature conditions.

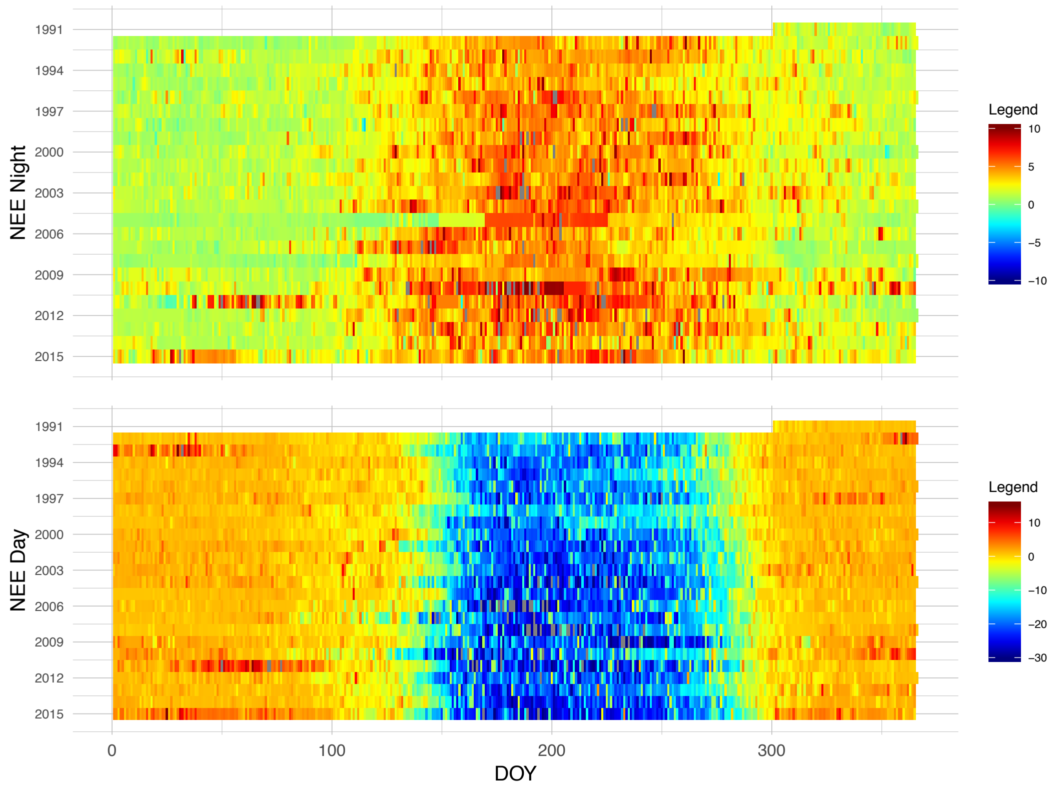

Figure A2. HF-EMS tower daily diurnal averages

866 *Appendix A.2. JERC-RD EC Flux Tower*

867 Recent historical mean daily fluxes of latent heat flux (LE) ($W\ m^{-2}$), ecosystem respiration
868 ($\mu mol\ CO_2\ m^{-2}$), and NEE ($\mu mol\ C\ m^{-2}$) for the RD flux tower are shown in Figure A3.

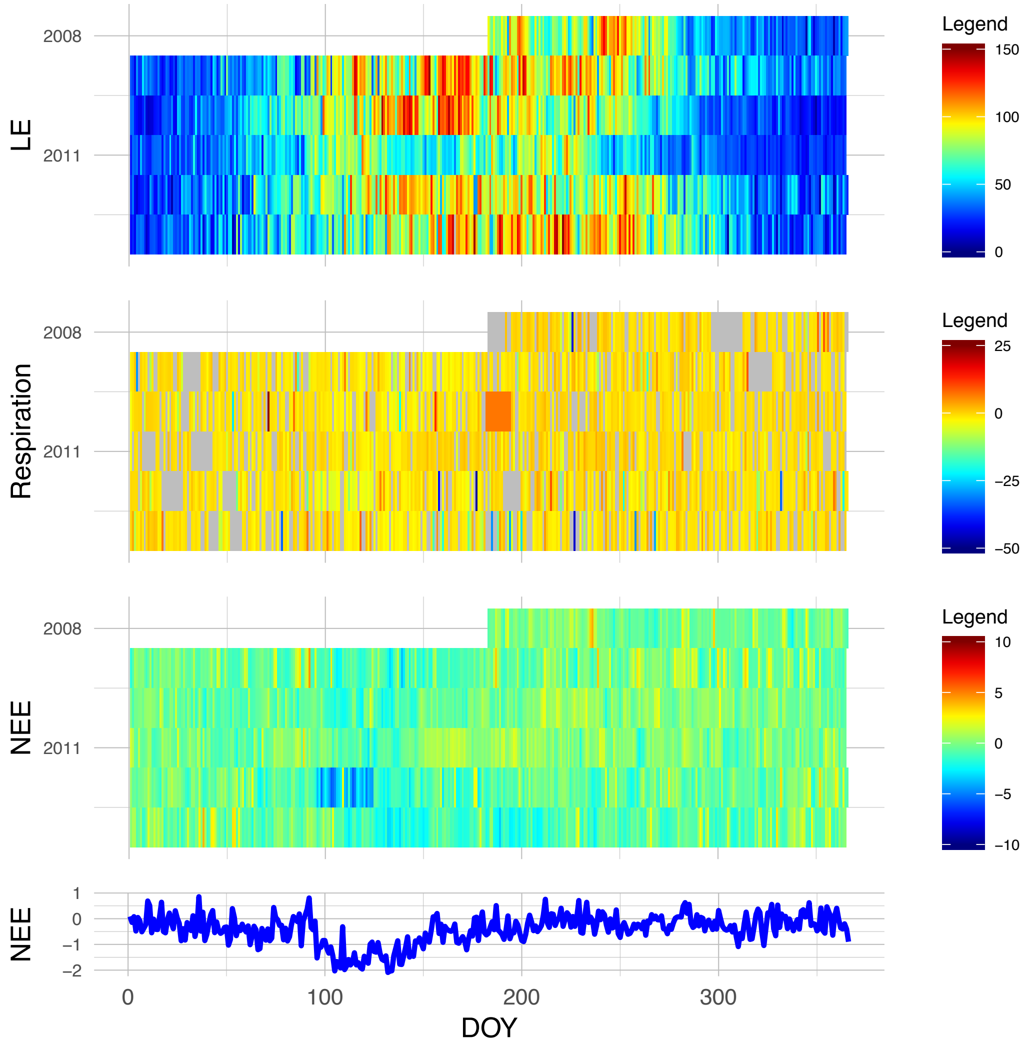

Figure A3. JERC-RD tower daily averages

869 Patterns of daytime and nighttime NEE are shown in Figure A4. Again, this was calculated by
870 taking daily mean NEE values for three-hour windows surrounding noon and midnight, respectively
871 (1100-1300 and 2300-0100 hours).

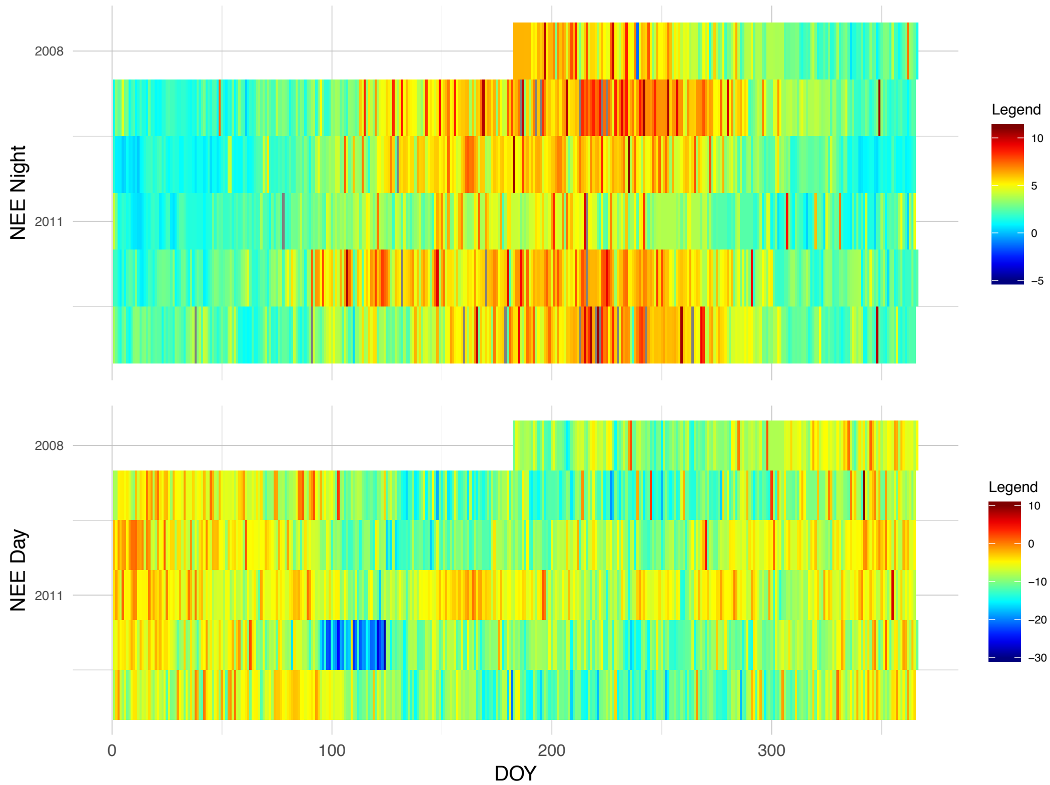

Figure A4. JERC-RD tower daily diurnal averages

872 ## Appendix B. Site maps

873 Below, we provide maps of the two research sites for reference. First is the HF-EMS EC flux tower
874 with landcover classes Figure A5.

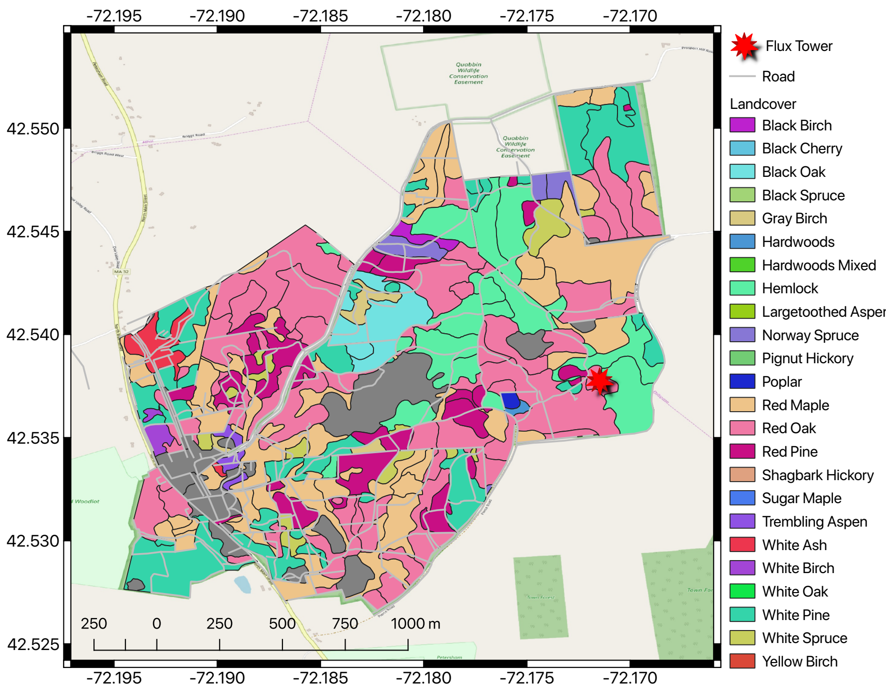

Figure A5. HF-EMS flux tower and landcover classes

875 Next is the JERC-RD flux tower with landcover classes Figure A6.

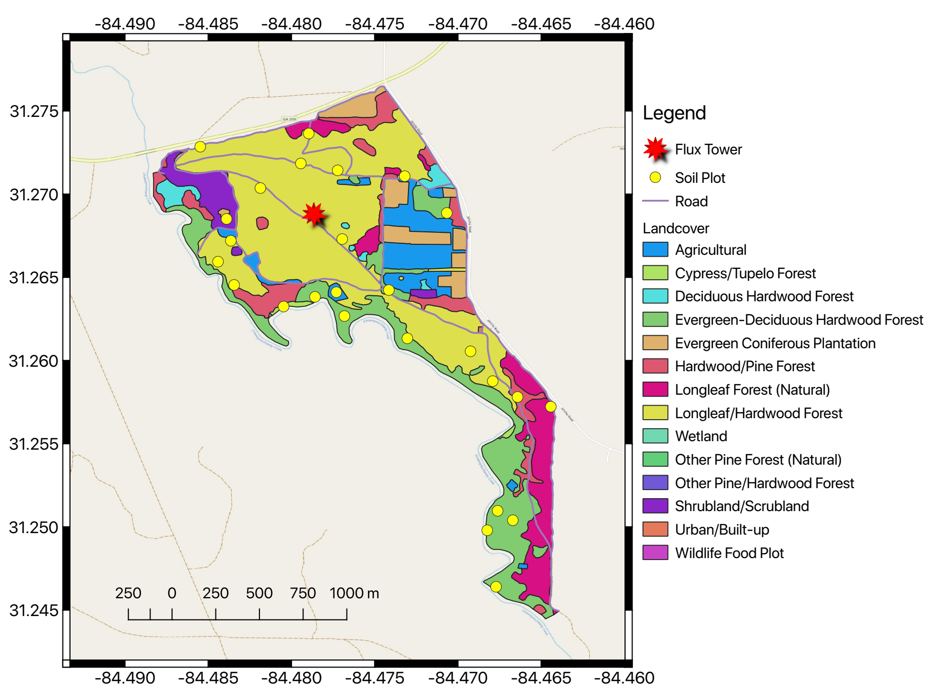

Figure A6. JERC-RD flux tower and landcover classes

Appendix C. Model Parameters

Appendix C.1. HF-EMS

Appendix C.1.1. PPA-SiBGC

Table A1. Species crown allometry parameters

Species	Type	h_{coeff}	cr_1	cr_2	cd
ACPE	adult	0.063	0.108	1	0.490
ACRU	adult	0.063	0.108	1	0.490
BEAL	adult	0.063	0.109	1	0.540
BELE	adult	0.024	0.109	1	0.540
BEPO	adult	0.063	0.109	1	0.540
FAGR	adult	0.035	0.152	1	0.664
FRAM	adult	0.056	0.095	1	0.319
PIGL	adult	0.033	0.087	1	0.413
PIRE	adult	0.033	0.087	1	0.413
PIST	adult	0.033	0.087	1	0.413
PRSE	adult	0.045	0.116	1	0.370
QURU	adult	0.042	0.119	1	0.413
QUVE	adult	0.042	0.119	1	0.413
TSCA	adult	0.024	0.100	1	0.846
ACPE	sapling	0.062	0.107	1	0.580
ACRU	sapling	0.063	0.108	1	0.490
BEAL	sapling	0.063	0.109	1	0.540
BELE	sapling	0.024	0.109	1	0.540
BEPO	sapling	0.063	0.109	1	0.540
FAGR	sapling	0.035	0.152	1	0.664
FRAM	sapling	0.056	0.095	1	0.319
PIGL	sapling	0.033	0.087	1	0.413
PIRE	sapling	0.033	0.087	1	0.413
PIST	sapling	0.033	0.087	1	0.413
PRSE	sapling	0.045	0.116	1	0.370
QURU	sapling	0.042	0.119	1	0.413
QUVE	sapling	0.042	0.119	1	0.413
TSCA	sapling	0.024	0.100	1	0.846

Table A2. Species biomass equation parameters

Species	$b0$	$b1$	f_{stem}	f_{branch}	f_{leaf}	f_{root}	f_{soil}
ACPE	−2.047	2.385	0.700	0.230	0.070	0.240	0.680
ACRU	−2.047	2.385	0.700	0.230	0.070	0.240	0.680
BEAL	−1.810	2.348	0.700	0.230	0.070	0.240	0.680
BELE	−1.810	2.348	0.700	0.230	0.070	0.240	0.680
BEPO	−2.227	2.451	0.700	0.230	0.070	0.240	0.680
FAGR	−2.070	2.441	0.700	0.230	0.070	0.240	0.680
FRAM	−1.838	2.352	0.700	0.230	0.070	0.240	0.680
PIGL	−2.136	2.323	0.700	0.230	0.070	0.240	0.680
PIRE	−2.618	2.464	0.700	0.230	0.070	0.240	0.680
PIST	−2.618	2.464	0.700	0.230	0.070	0.240	0.680
PRSE	−2.212	2.413	0.700	0.230	0.070	0.240	0.680
QURU	−2.070	2.441	0.700	0.230	0.070	0.240	0.680
QUVE	−2.070	2.441	0.700	0.230	0.070	0.240	0.680
TSCA	−2.348	2.388	0.700	0.230	0.070	0.240	0.680

Table A3. Biomass carbon fraction parameters

f_{stem}	f_{branch}	f_{leaf}	f_{root}	f_{soil}
0.500	0.500	0.500	0.500	0.143

Table A4. Species DBH increment parameters

Species	Type	I_{DBH}
ACPE	adult	0.277
ACRU	adult	0.312
BEAL	adult	0.280
BELE	adult	0.198
BEPO	adult	0.103
FAGR	adult	0.303
FRAM	adult	0.149
PIGL	adult	0.274
PIRE	adult	0.390
PIST	adult	0.277
PRSE	adult	0.120
QURU	adult	0.420
QUVE	adult	0.322
TSCA	adult	0.563
ACPE	sapling	0.895
ACRU	sapling	0.269
BEAL	sapling	0.520
BELE	sapling	0.201
BEPO	sapling	0.300
FAGR	sapling	0.530
FRAM	sapling	0.500
PIGL	sapling	0.353
PIRE	sapling	0.350
PIST	sapling	0.350
PRSE	sapling	0.200
QURU	sapling	0.098
QUVE	sapling	0.100
TSCA	sapling	0.509

Table A5. Species mortality parameters

Species	Type	$p_{mortality}$
ACPE	adult	0.115
ACRU	adult	0.030
BEAL	adult	0.035
BELE	adult	0.009
BEPO	adult	0.032
FAGR	adult	0.015
FRAM	adult	0.004
PIGL	adult	0.074
PIRE	adult	0.023
PIST	adult	0.010
PRSE	adult	0.009
QURU	adult	0.007
QUVE	adult	0.001
TSCA	adult	0.022
ACPE	sapling	0.001
ACRU	sapling	0.873
BEAL	sapling	0.001
BELE	sapling	0.667
BEPO	sapling	0.001
FAGR	sapling	0.354
FRAM	sapling	0.001
PIGL	sapling	0.001
PIRE	sapling	0.001
PIST	sapling	0.001
PRSE	sapling	0.001
QURU	sapling	0.001
QUVE	sapling	0.001
TSCA	sapling	0.821

Table A6. Species fecundity parameters

Species	Fecundity
ACPE	2
ACRU	29
BEAL	16
BELE	8
BEPO	2
FAGR	11
FRAM	5
PIGL	3
PIRE	3
PIST	11
PRSE	8
QURU	29
QUVE	9
TSCA	17

Table A7. Species C:N ratio parameters

Species	CN_{stem}	CN_{branch}	CN_{leaf}	CN_{litter}	CN_{root}	CN_{soil}
ACPE	548.590	71.460	30.460	58.800	68.548	23.087
ACRU	548.590	71.460	30.460	58.800	68.548	23.087
BEAL	548.590	71.460	22.420	58.800	68.548	23.087
BELE	548.590	71.460	21.200	58.800	68.548	23.087
BEPO	548.590	71.460	21.560	58.800	68.548	23.087
FAGR	548.590	71.460	22.420	58.800	68.548	23.087
FRAM	548.590	71.460	21.910	58.800	68.548	23.087
PIGL	548.590	71.460	38	58.800	68.548	23.087
PIRE	548.590	71.460	33	58.800	68.548	23.087
PIST	548.590	71.460	38	58.800	68.548	23.087
PRSE	548.590	71.460	21.500	58.800	68.548	23.087
QURU	548.590	71.460	21.920	58.800	68.548	23.087
QUVE	548.590	71.460	21.920	58.800	68.548	23.087
TSCA	548.590	71.460	42.520	58.800	68.548	23.087

879 Appendix C.1.2. LANDIS-II NECN

Table A8. NECN adjustment parameters

Parameter	Value
p_{est} modifier	0.1
$N_{mineral}$ initial	3.0
$Fuels_{fine}$ initial	0.1
N_{atmos} slope	0.007
N_{atmos} intercept	0.011
$Latitude_{deg}$	43.3
$r_{denitrification}$	0.001
r_{decay} surface	0.65
r_{decay} SOM1	1.0
r_{decay} SOM2	0.125
r_{decay} SOM3	0.0002

Table A9. NECN maximum LAI parameters

$Class_{shade}$	LAI_{max}
1	1
2	2.5
3	3.5
4	6
5	8

Table A10. NECN light establishment parameters

$Class_{shade}$	$Shade_0$	$Shade_1$	$Shade_2$	$Shade_3$	$Shade_4$	$Shade_5$
1	1	1	0.25	0.1	0	0
2	0.5	0.5	1	0.25	0.1	0
3	0.1	0.5	1	1	0.5	0.1
4	0.1	0.25	0.5	0.5	1	0.25
5	0	0.1	0.25	0.25	0.5	1

Table A11. NECN species parameters

Species	PFT	N_{fix}	GDD_{min}	GDD_{max}	T_{min}	D_{max}	$Long_{leaf}$	R_{epi}	L_{leaf}	L_{root_f}	L_{wood}	L_{root_c}	CN_{leaf}	CN_{root_f}	CN_{wood}	CN_{root_c}	CN_{litter}	$ANPP_{max}$	B_{max}
ACRU	3	N	1260	6600	-18	0.23	1	N	0.183	0.334	0.125	0.312	28.20	26	565	50	55	440	25000
QURU	2	N	1100	4571	-17	0.2025	1	N	0.249	0.334	0.225	0.303	18.50	58	398	113	32	380	25000

Table A12. Functional group parameters

PFT	Index	T_{mean}	T_{max}	T_{shape}	T_{shape}	f_Cf	$BTOLAI$	$kLAI$	LAI_{max}	$PPRPTS_2$	$PPRPTS_3$	$r_{decay}w$	m_{wood}	m_{shape}	$drop_{month}$	$f_{root}c$	$f_{root}f$
Oaks	2	25	40	1.5	2.5	0.6	-0.9	10000	9	0.1	0.8	0.5	0.0006	15	9	0.2	0.5
NorthHardwoods	3	25	40	1.5	2.5	0.6	-0.9	7000	10	1.5	0.96	0.7	0.0006	15	9	0.2	0.5

Table A13. Fire reduction parameters; inactive

$Class_{severity}$	$Reduction_{wood}$	$Reduction_{litter}$	$Reduction_{SOM}$
1	0.0	0.5	1.0
2	0.05	0.75	1.0
3	0.2	1.0	1.0
4	0.5	1.0	1.0
5	0.8	1.0	1.0

Table A14. Harvest reduction parameters; inactive

Class	$Reduction_{wood}$	$Reduction_{litter}$	$Reduction_{SOM}$	$Removal_{leaf}$	$Removal_{wood}$
HandThinning	0.05	1.0	1.0	1.0	1.0
MechThinning	0.05	1.0	1.0	0.85	1.0

Table A15. Species parameters; only ACRU and QURU were simulated

Species	Longevity	Maturity	T_{shade}	T_{fire}	D_{eff}	D_{max}	p_{veg}	S_{min}	S_{max}	R_{fire}
ABBA	200	25	5	1	30	160	0	0	0	none
ACRU	235	5	4	1	100	200	0.75	0	150	none
ACSA	300	40	5	1	100	200	0.1	0	60	none
BEAL	300	40	3	2	100	400	0.1	0	180	none
BELE	250	40	4	2	100	400	0.1	0	0	none
BEPA	150	40	4	2	100	600	0.75	0	150	none
BEPO	150	40	4	2	100	400	0.1	0	0	none
CAGL	200	30	3	2	50	100	0.25	0	200	resprout
FAGR	350	10	5	1	30	300	0.4	10	200	resprout
FRAM	300	30	2	1	70	140	0.1	0	70	none
FRNI	150	30	4	2	200	2000	0.8	10	140	resprout
LALA	180	35	2	2	100	400	0.2	0	0	none
OSVI	110	25	4	2	100	200	0.15	0	100	resprout
PIGL	300	25	3	2	30	200	0	0	0	none
PIMA	215	30	3	3	79	158	0	0	0	none
PIRU	350	15	5	2	80	125	0	0	0	none
PIRE	250	15	2	4	100	275	0.1	0	20	none
PIRI	200	10	2	4	90	150	0.5	10	100	resprout
PIST	400	25	3	3	60	210	0	0	0	none
POBA	150	10	1	2	100	200	0.8	10	80	resprout
POGR	110	20	1	1	1000	5000	0.9	0	100	resprout
POTR	110	20	1	1	1000	5000	0.9	0	100	resprout
PRSE	200	10	2	3	100	200	0.5	20	90	resprout
QUAL	400	25	3	2	30	800	0.1	20	200	resprout
QUCO	150	20	2	3	50	100	0.5	20	100	resprout
QUPR	300	20	3	3	50	150	0.5	10	200	resprout
QURU	250	30	3	2	30	800	0.5	20	200	resprout
QUVE	120	20	3	2	70	150	0.1	20	90	resprout
THOC	800	30	2	1	45	100	0.5	0	200	none
TIAM	250	15	4	1	75	150	0.8	10	240	resprout
TSCA	500	20	5	2	30	100	0	0	0	none
ULAM	85	20	4	2	90	400	0.3	5	70	resprout

880 *Appendix C.2. JERC-RD*

881 Appendix C.2.1. PPA-SiBGC

Table A16. Species crown allometry parameters

Species	Type	h_{coeff}	$cr1$	$cr2$	cd
PIPA	adult	0.033	0.087	1	0.413
QUIN	adult	0.042	0.119	1	0.413
QUNI	adult	0.042	0.119	1	0.413
QUVI	adult	0.042	0.119	1	0.413
PIPA	sapling	0.033	0.087	1	0.413
QUIN	sapling	0.042	0.119	1	0.413
QUNI	sapling	0.042	0.119	1	0.413
QUVI	sapling	0.042	0.119	1	0.413

Table A17. Species biomass equation parameters

Species	$b0$	$b1$	f_{stem}	f_{branch}	f_{leaf}	f_{root}	f_{soil}
PIPA	-3.051	2.647	0.700	0.230	0.070	0.240	0.680
QUIN	-2.070	2.441	0.700	0.230	0.070	0.240	0.680
QUNI	-2.070	2.441	0.700	0.230	0.070	0.240	0.680
QUVI	-2.070	2.441	0.700	0.230	0.070	0.240	0.680

Table A18. Biomass carbon fraction parameters

f_{stem}	f_{branch}	f_{leaf}	f_{root}	f_{soil}
0.500	0.500	0.500	0.500	0.143

Table A19. Species DBH increment parameters

Species	Type	I_{DBH}
PIPA	adult	0.261
QUIN	adult	0.119
QUNI	adult	0.994
QUVI	adult	0.276
PIPA	sapling	0.197
QUIN	sapling	0.100
QUNI	sapling	0.440
QUVI	sapling	0.271

Table A20. Species mortality parameters

Species	Type	$p_{mortality}$
PIPA	adult	0.001
QUIN	adult	0.001
QUNI	adult	0.001
QUVI	adult	0.001
PIPA	sapling	0.174
QUIN	sapling	0.333
QUNI	sapling	0.143
QUVI	sapling	0.111

Table A21. Species fecundity parameters

Species	Fecundity
PIPA	2
QUIN	0
QUNI	0
QUVI	0

Table A22. Species C:N ratio parameters

Species	CN_{stem}	CN_{branch}	CN_{leaf}	CN_{litter}	CN_{root}	CN_{soil}
PIPA	133.721	133.721	255.103	255.103	133.721	23.087
QUIN	96.370	96.370	85.259	85.259	96.370	23.087
QUNI	96.370	96.370	85.259	85.259	96.370	23.087
QUVI	96.370	96.370	85.259	85.259	96.370	23.087

882 Appendix C.2.2. LANDIS-II NECN

Table A23. NECN adjustment parameters

Parameter	Value
p_{est} modifier	0.4
$N_{mineral}$ initial	0.5
$Fuels_{fine}$ initial	0.1
N_{atmos} slope	0.004
N_{atmos} intercept	0.017
$Latitude_{deg}$	31.220731
$r_{denitrification}$	0.02
r_{decay} surface	0.70
r_{decay} SOM1	0.81
r_{decay} SOM2	0.05
r_{decay} SOM3	0.00006

Table A24. NECN maximum LAI parameters

$Class_{shade}$	LAI_{max}
1	1
2	2.5
3	3.5
4	6
5	8

Table A25. NECN light establishment parameters

$Class_{shade}$	$Shade_0$	$Shade_1$	$Shade_2$	$Shade_3$	$Shade_4$	$Shade_5$
1	1	1	0.25	0.1	0	0
2	0.5	0.5	1	0.25	0.1	0
3	0.1	1	1	1	0.5	0.1
4	0.1	0.25	0.5	0.5	1	0.25
5	0	0.1	0.25	0.25	0.5	1

Table A26. NECN species parameters

Species	PFT	N_{fix}	GDD_{min}	GDD_{max}	T_{min}	D_{max}	$Long_{leaf}$	R_{epi}	L_{leaf}	L_{root_f}	L_{wood}	L_{root_c}	CN_{leaf}	CN_{root_f}	CN_{wood}	CN_{root_c}	CN_{litter}	$ANPP_{max}$	B_{max}
QUIN	2	N	3915	7000	1	0.423	1	N	0.293	0.23	0.23	0.35	24	48	500	333	55	250	15000
QULA	2	N	3915	7000	1	0.423	1	N	0.293	0.23	0.23	0.35	24	48	500	333	55	250	15000
PIPA	1	N	3915	7000	1	0.423	2	N	0.2	0.2	0.35	0.35	50	50	380	170	100	500	15000

Table A27. Functional group parameters

PFT	Index	T_{mean}	T_{max}	T_{shape}	T_{shape}	f_{C_f}	$BTOLAI$	$kLAI$	LAI_{max}	$PPRPTS_2$	$PPRPTS_3$	r_{decay_w}	m_{wood}	m_{shape}	$month_{drop}$	f_{root_c}	f_{root_f}
Pine	1	28	45	3.0	2.5	0.37	-0.9	2000	10	1	0.8	0.6	0.001	15	9	0.31	0.56
Oaks	2	27	45	2.2	2.5	0.5	-0.9	2000	20	0.1	0.75	0.6	0.001	15	9	0.21	0.59

Table A28. Fire reduction parameters; inactive

$Class_{severity}$	$Reduction_{wood}$	$Reduction_{litter}$	$Reduction_{SOM}$
1	0.0	0.5	1.0
2	0.05	0.75	1.0
3	0.2	1.0	1.0
4	0.5	1.0	1.0
5	0.8	1.0	1.0

Table A29. Harvest reduction parameters; inactive

$Class_{severity}$	$Reduction_{wood}$	$Reduction_{litter}$	$Reduction_{SOM}$	$Removal_{leaf}$	$Removal_{wood}$
HandThinning	0.05	1.0	1.0	1.0	1.0
MechThinning	0.05	1.0	1.0	0.85	1.0

Table A30. Species parameters

Species	Longevity	Maturity	T_{shade}	T_{fire}	D_{eff}	D_{max}	p_{veg}	S_{min}	S_{max}	R_{fire}
QUIN	150	10	4	5	50	3000	0.75	5	40	resprout
QULA	150	20	4	3	50	3000	0.75	5	40	resprout
PIPA	400	20	1	5	20	200	0.0	0	5	none